

Urban Incident Prediction with Graph Neural Networks: Integrating Government Ratings and Crowdsourced Reports

Sidhika Balachandar^{1*}, Shuvom Sadhuka², Bonnie Berger², Emma Pierson³, Nikhil Garg⁴

¹ Department of Computer Science, Cornell Tech

² CSAIL, Massachusetts Institute of Technology

³ Department of EECS, UC Berkeley

⁴ Department of Operations Research, Jacobs Technion-Cornell Institute Cornell Tech

Abstract

Graph neural networks (GNNs) are widely used in urban spatiotemporal forecasting, such as predicting infrastructure problems. In this setting, government officials wish to know in which neighborhoods incidents like potholes or rodent issues occur. The true state of incidents (e.g., street conditions) for each neighborhood is observed via government inspection *ratings*. However, these ratings are only conducted for a sparse set of neighborhoods and incident types. We also observe the state of incidents via crowdsourced *reports*, which are more densely observed but may be biased due to heterogeneous reporting behavior. First, for such settings, we propose a multiview, multioutput GNN-based model that uses both unbiased rating data and biased reporting data to predict the true latent state of incidents. Second, we investigate a case study of New York City urban incidents and collect, standardize, and make publicly available a dataset of 9,615,863 crowdsourced reports and 1,041,415 government inspection ratings over 3 years and across 139 types of incidents. Finally, we show on both real and semi-synthetic data that our model can better predict the latent state compared to models that use only reporting data or models that use only rating data, especially when rating data is sparse and reports are predictive of ratings. We also quantify demographic biases in crowdsourced reporting, e.g., higher-income neighborhoods report problems at higher rates. Our analysis showcases a widely applicable approach for latent state prediction using heterogeneous, sparse, and biased data.

Model — https://github.com/sidhikabalachandar/nyc_urban_incident_model

Dataset — https://github.com/sidhikabalachandar/nyc_urban_incident_data

Introduction

Graph neural networks (GNNs) have emerged as powerful and expressive models for making predictions on graph-structured data, including for urban applications such as air quality monitoring, forecasting traffic flows, predicting housing prices, and modeling the spread of epidemics (Xie et al. 2019; Roy et al. 2021; Brimos et al. 2023; Yu et al. 2023; Zhan and Datta 2024). We study urban planning—i.e., the design and regulation of land use, infrastructure, and

resources for sustainable and efficient cities. In this setting, government officials often wish to know where incidents like rodent infestations or floods truly occur so they can make downstream resource allocation decisions; however, ground truth is often unobserved. GNNs are a powerful prediction tool, as they can encode spatial correlations of the ground-truth states across nodes in a graph (e.g., neighborhoods in a city) as well as across hundreds of types of incidents. For example, if a flood has occurred in one neighborhood, the adjacent neighborhoods are also likely to be flooded and might also experience related incidents like street damage.

Estimating latent ground truth for the hundreds of types of incidents in a city is challenging. Two sources of information are often used, each with its limitations. First, we observe the ground-truth state via *government inspections*, which generate *ratings* for neighborhoods. Importantly, these inspections are only conducted for some incident types and neighborhoods and thus ratings are sparsely observed. For example, New York City conducts street inspections for every street and rates them from 1-10, but each street is only rated about once every year. Second, we observe biased proxies of the latent state via crowdsourced *reports* of incidents. Compared to ratings, indicators of whether a report is observed are available for every incident type and neighborhood; e.g., we process data from 9,615,863 reports across 3 years. These data characteristics, where both sparsely observed ground truth data and frequently observed biased data are available, are common in many prediction tasks in urban planning and other domains.

A challenge is that learning only from reporting data leads to biased predictions. Previous work has established that underreporting is pervasive and heterogeneous (O’Brien, Sampson, and Winship 2015; O’Brien et al. 2017; Clark et al. 2020; Kontokosta and Hong 2021; Agostini, Pierson, and Garg 2024; Liu, Bhandaram, and Garg 2024); in different neighborhoods that face similar incidents, residents often *report* those incidents at different rates. This bias presents an identifiability issue; if one neighborhood logs more reports than another, it is unclear whether the former has a worse ground truth, or if given the same ground truth, the latter is less likely to report. As a result, for example, Casey, Wilson, and Yokum (2018) found that in Washington, D.C., crowdsourced reports on rodents did not accurately predict the outcome of inspections. Moreover, differences in re-

*Correspondance to sidhikab@cs.cornell.edu or ngarg@cornell.edu

porting often correlate with demographics, so learning only from reporting data risks introducing decisionmaking disparities against underserved populations (Agostini, Pierson, and Garg 2024; Liu, Bhandaram, and Garg 2024).

In summary, we define the novel task of prediction in urban settings with the following data characteristics: (i) high dimensionality, i.e., data across hundreds of incident types; (ii) frequently observed biased reporting data; and (iii) sparsely observed ground-truth rating data. We make the following contributions:

- We propose a multiview, multioutput GNN-based model for this task. As summarized in Figure 1, we jointly model the true latent state and the probability of a report for each neighborhood across all incident types. Using both sparsely observed ground-truth rating data and frequently observed biased reporting data, we train our model to simultaneously predict ground-truth ratings using learned node and type embeddings and infer how the likelihood of reporting varies by demographics, conditional on ground-truth. Our model’s novel contribution lies in adapting GNN architectures for biased data settings by connecting multi-view datasets through a multi-output loss function. Our model is available here: https://github.com/sidhikabalachandar/nyc_urban_incident_model.
- We investigate a case study of New York City urban incidents. We create a heterogeneous dataset of reports and ratings. We source reports from New York City 311 complaints (crowdsourced reports), using a total of 9,615,863 reports made across 139 complaint types over three years. We combine this with ground-truth ratings sourced from 1,041,415 government inspections across 5 complaint types in the same time frame. We remove inspection ratings likely made in response to reports, mitigating reporting bias. Our produced dataset presents two advantages. First off, our dataset is highly heterogeneous, and contains data across different time periods, nodes, and types. Through various train/test splits, our data can be used to evaluate model performance on unseen time periods, nodes, and incident types. A second advantage of this dataset is that new data – via reports and government inspections – for a large set of incident types and locations is available daily, serving as an ideal setting in which to study distribution shifts over time and providing an automatic source of uncontaminated test sets. We make our processed data and code publicly available to enable further research on this task. Our data is available here: https://github.com/sidhikabalachandar/nyc_urban_incident_data.
- We show that our approach can predict the ground-truth inspection ratings and quantify reporting biases. In both semi-synthetic and real data, we find that jointly using the sparsely observed ground-truth rating data and the frequently observed biased reporting data outperforms using reporting data alone (predicted ratings are $1.8\times$ more correlated on semi-synthetic data and $5.3\times$ more correlated on real data) or using rating data alone, especially when ratings are sparsely observed. Finally, we

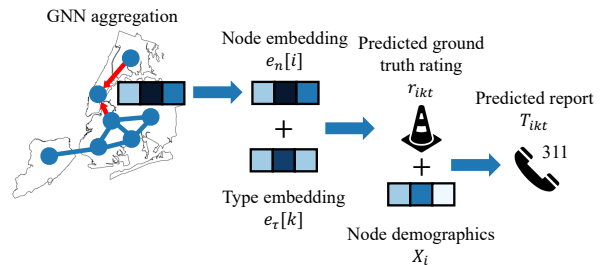


Figure 1: *Model*. We use a GNN-based model to estimate inspection ratings and reports of incidents. We model inspection ratings r_{ikt} using node i ’s learned embedding $e_n[i]$ and type k ’s learned embedding $e_\tau[k]$. We model reports T_{ikt} as a function of the rating r_{ikt} and demographics X_i .

quantify the biases in the reporting data, finding that conditional on ground-truth, neighborhoods with higher population density, higher median income, higher proportion of the population with a bachelor’s degree, older residents, higher proportion of white residents, and worse ground-truth states all report incidents at higher rates.

More broadly, our approach contributes to more equitable and responsible urban AI applications. Explicit modeling of differential reporting across groups may be necessary to make resource allocation decisions based on more accurate representations of ground truth. This can help ensure that underserved communities receive appropriate resources, despite potential underreporting of incidents. Quantifying reporting biases also creates transparency about which communities may be underrepresented in traditional data collection methods, enabling targeted outreach efforts to increase civic participation across all demographics.

Although our primary application is urban crowdsourcing, our approach is applicable to other prediction tasks where both sparsely observed ground-truth data and frequently observed biased data are available. Specific application areas include other urban challenges (such as estimating air quality using both resident reports and sparse sensor measurements (Sarto et al. 2016; Samal, Babu, and Das 2022)) and spatiotemporal processes (such as epidemic forecasting using both internet search data and sparse official health reports (Kapoor et al. 2020; Hacker et al. 2022; Tomy et al. 2022; Wang et al. 2022a; Yu et al. 2023)).

Related work

Our work is broadly related to literature on (i) prediction in urban settings, (ii) the use of GNNs in biased data settings, and (iii) the use of GNNs for spatiotemporal modeling.

Predicting urban incidents: A large literature seeks to predict urban incidents, such as flooding, infrastructure quality, and crime (Budde et al. 2014; O’Brien, Sampson, and Winship 2015; Lum and Isaac 2016; Sarto et al. 2016; Wang et al. 2017; Hu et al. 2018; Mosavi, Ozturk, and Chau 2018; Yu, Yin, and Zhu 2018; Gómez et al. 2019; Pan et al. 2019; Xie et al. 2019; Clark et al. 2020; Jiménez-Jiménez et al. 2020; Kontokosta and Hong 2021; Agonafir et al. 2022;

Hacker et al. 2022; Mauerman et al. 2022; Farahmand, Xu, and Mostafavi 2023; Zaouche and Bode 2023; Agostini, Pierson, and Garg 2024; Gao et al. 2024). A challenge is that data is biased often due to human behavior (Lum and Isaac 2016; Wang et al. 2017; Clark et al. 2020; Kontokosta and Hong 2021; Agostini, Pierson, and Garg 2024; Gao et al. 2024; Liu, Bhandaram, and Garg 2024). With selection bias, crowdsourced reports may not fully represent ground-truth states. For example, prior work on urban incident crowdsourcing has quantified underreporting of floods using spatiotemporal models (Agostini, Pierson, and Garg 2024) and has quantified the geographic and demographic patterns of underreporting (Wang et al. 2017; Clark et al. 2020; Kontokosta and Hong 2021; Gao et al. 2024; Liu, Bhandaram, and Garg 2024). Disparities in incident reporting rates lead to downstream inequities in resource allocation, so understanding the patterns of underreporting is crucial (Liu, Bhandaram, and Garg 2024; Liu and Garg 2024). Especially notable in relation to our work is that of Casey, Wilson, and Yokum (2018), who show in Washington, D.C., that 311 reports alone are poor predictors of ground-truth ratings.

Our contribution: Existing works in this area typically consider only one or a few related incident types (e.g., floods or rodents); thus a novel contribution of our model is its ability to learn and make predictions for more than a hundred 311 complaint types. Additionally, many related works use statistical models that make strict assumptions (Agostini, Pierson, and Garg 2024), whereas our GNN-based model presents a flexible approach to modeling spatial correlation in urban incident settings across a high-dimensional dataset. Finally, we create a heterogeneous spatial dataset with biased outcome data. We hope this data can be used by other researchers to study data bias in urban applications.

Using GNNs for biased data: A common approach to addressing selection bias in GNNs is *graph-based semi-supervised learning*, which uses two primary methods to infer labels for unlabeled datapoints (Song et al. 2023): graph regularization, which propagates labels from labeled to unlabeled nodes using the graph structure (Zhou et al. 2003; Zhu, Ghahramani, and Lafferty 2003; Belkin, Niyogi, and Sindhwani 2006; Dai, Aggarwal, and Wang 2021; Verma et al. 2021; Li, Yin, and Chen 2023; Qian et al. 2023; Zhou et al. 2024), and graph embedding, which generates low-dimensional representations for nodes to infer labels for unlabeled nodes (Perozzi, Al-Rfou, and Skiena 2014; Tang et al. 2015; Grover and Leskovec 2016; Li, Xiong, and Hoi 2021; Sharma and Jones 2023). Other recent works have generated pseudo-labels using softmax predictions (Arazo et al. 2020), curriculum learning (Zhang et al. 2021), and a combination of entropy based filtering and contrastive learning (Wang et al. 2022b). Other GNN approaches to biased data include causal regularization (Kyono, Zhang, and van der Schaar 2020; Wang et al. 2022a; Wu et al. 2023) and graph attention (Wang et al. 2019; Brody, Alon, and Yahav 2022; Sui et al. 2022).

Our contribution: These related works discuss how to effectively train GNNs on sparsely labeled data (e.g., inspection ratings) by generating proxy labels for the unlabeled

datapoints. We extend this literature by identifying another approach to obtaining proxy labels: using data from a frequently observed source that is a biased proxy for the target of interest (e.g., whether or not a report is made is a biased proxy of the ground-truth rating). We also learn the relationship between the biased data and ground truth.

Using GNNs for spatiotemporal modeling: GNNs are a natural fit for high-dimensional spatiotemporal modeling in applications like traffic forecasting, epidemic forecasting, and molecular dynamics (Kapoor et al. 2020; Roy et al. 2021; Wang et al. 2022a,c; He et al. 2023; Pineda et al. 2023; Wu et al. 2024). Several works also design ways to encode spatiotemporal information in GNNs, including kriging convolutional networks (Appleby, Liu, and Liu 2020), positional encoders (Klemmer, Safir, and Neill 2023), and inductive kriging (Wu et al. 2021). Non-GNN-based spatiotemporal modeling, including Bayesian models, clustering, and matrix factorization models, have also been used for urban issues like infrastructure monitoring (Budde et al. 2014), crime (Hu et al. 2018), urban flow (Pan et al. 2019), air pollution (Sarto et al. 2016), and pedestrian traffic (Zaouche and Bode 2023).

Our study also relates to literature on *multi-view GNNs*, which integrate information from multiple datasets or views to improve representation learning and predictive performance (Shao et al. 2023; Cheng et al. 2018), and *multi-output GNNs*, which predict multiple outputs from a single graph by leveraging shared graph structure and correlations between the target outputs (Peng et al. 2022; Samal, Babu, and Das 2022).

Our contribution: Related works that use GNNs for spatiotemporal modeling have identified that learning only from proxy data (reports) results in biased predictions of ground truth. We extend this literature by identifying an approach to improve predictions: additionally learning from sparse ground-truth data (inspection ratings). We show that our model, which uses both reporting and rating data, makes better predictions than a model trained only on biased reporting data, validating the efficacy of our approach.

Additionally, while multi-view and multioutput GNNs have been used for spatiotemporal tasks, prior work does not explicitly model biases or how different views or outputs connect to each other. Therefore our model’s novel methodological contribution lies in adapting GNN architectures for biased data settings through its utilization of multi-view datasets and implementation of a multi-output loss function.

Setting and data

We now describe our setting. The goal is to estimate the ground-truth state of the hundreds of types of incidents that occur in a city (e.g., rodents, floods, etc.). There are two sources of data for this task: frequently observed biased crowdsourced *reporting* data and sparsely observed unbiased inspection *rating* data.

This setting is commonplace in urban prediction tasks and other related settings. In environmental monitoring, ratings may be geographically sparse sensor measurements of air quality and reports may be resident reports of air quality. In

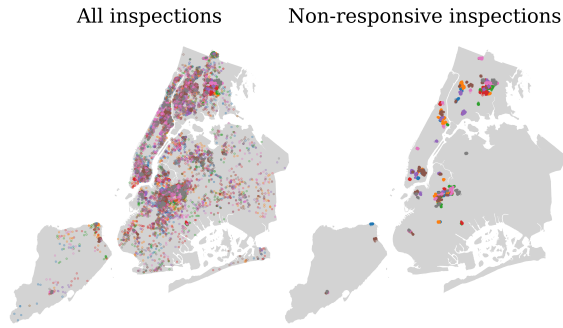


Figure 2: *Data processing.* We process the rodent ratings to remove all inspections triggered by crowdsourced reports. There are two types of inspections: (i) inspections responding to reports and (ii) non-responsive inspections conducted block-by-block in a scheduled manner (NYC Open Data 2024e). We apply a heuristic to keep only the non-responsive inspections. This figure shows the location of rodent inspections for the first 8 weeks of 2023. While the responsive inspections are distributed throughout the city (left), the non-responsive inspections show clear block-by-block clustering (right).

epidemic forecasting, ratings may be sparse health reports and reports may be internet searches (Chang, Fourney, and Horvitz 2024; Bauer and Aschenbruck 2018).

To our knowledge, prior urban prediction work has not considered the dual challenges and benefits of jointly learning from this available data—one reason is the lack of processed data, combining reports and ratings across types. We formalize this setting and provide large-scale preprocessed data composed of 9,615,863 crowdsourced reports across 139 incident types and 1,041,415 government inspection ratings across 5 incident types. Additional details on the data are provided in the appendix data section.

Dataset overview: Using the observed data sources, we create a multiview dataset of ratings and reports from New York City. We analyze all Census tracts¹ with valid demographic information (2292 tracts). We use all complaint types that receive at least one report for greater than 0.1% of all Census tract/week pairs. We study all data in the three year period from 2021 - 2023. We discretize time into 157 weeks. The main novel contribution of our dataset is its heterogeneity in combining reporting and inspection rating data. Our dataset consists of data across different time periods, nodes, and types. Through various train/test splits, our data can be used to evaluate model performance on unseen time periods, nodes, and incident types. Moreover, compared to related work on urban incident prediction, our data represents the most diverse set of types. In particular, many related works only analyze *one or a few* incident types or government agencies (Agostini, Pierson, and Garg 2024;

¹A Census tract is a geographic region defined by the U.S. Census Bureau to analyze population data. On average, each Census tract has thousands of inhabitants. There are 2326 total Census tracts in New York City.

Liu, Bhandaram, and Garg 2024; Liu and Garg 2024; Xu et al. 2017; Clark et al. 2020; Kontokosta, Hong, and Korsberg 2017; Agonafir et al. 2022; Casey, Wilson, and Yokum 2018). In contrast, our data represents the majority of available 311 incident types and agencies.

Observed data – Crowdsourced reports: We observe reports of incidents from New York City’s resident reporting system, NYC311 (NYC Open Data 2024a). We collect data from 9,615,863 reports. We transform reports into *indicators* of whether a report of a particular type was observed in a Census tract during a particular week.

Observed data – Inspection ratings: For some node, type, and week tuples, we also observe inspection ratings. We source ratings from city government inspections for various government services (e.g., street ratings, park ratings, etc.). A lower inspection rating indicates a worse true state; e.g., a street with a lower rating has more damage. We normalize (*z*-score) the inspection ratings for each type across time and nodes.

We collect ratings for five types: (i) street conditions (NYC Open Data 2023), (ii) park maintenance or facility conditions (NYC Open Data 2024d), (iii) rodents (NYC Open Data 2024e), (iv) food establishment/mobile food vendor/food poisoning (NYC Open Data 2024c), and (v) DCWP consumer complaints (NYC Open Data 2024b). We note that we *do not* observe ratings for every node/type/week tuple, and instead observe ratings for a sparse set of nodes, incident types, and weeks. A summary of the rating data, including the number of ratings and reports observed per type, is provided in Appendix Table 2. We collect data from 1,041,415 government inspections.

Our model treats government inspections as a source of unbiased data, and thus we ensure that the inspections are not susceptible to bias. Selection bias can occur if an inspection is conducted in response to a crowdsourced report. We process the inspection data to only use ratings *not* conducted in response to crowdsourced reports, as verified by the data dictionaries or by filtering out responsive inspections. For example, rodent inspections are conducted both block-by-block in a scheduled manner and in response to 311 reports; the data does not explicitly distinguish between these inspection reasons. Figure 2 (left) shows the spatiotemporal distribution of all rodent inspections in an eight-week period. We identify the non-responsive block-by-block inspections as those for which many other buildings in the same Census tract are inspected in the same week; see Figure 2 (right) for the identified non-responsive block-by-block inspections.

Matching ratings and reports to geographic units:

Next, we match government inspection ratings and crowdsourced reports to geographic regions and to each other. Each rating is for a fine-grained unit within a Census tract, e.g., street ratings are for street segments and rodent ratings are for buildings indicated by its Borough-Block-Lot (BBL) number. For node, incident type, and week tuples with an observed government inspection rating, we match the rating to its corresponding report. Thus, we provide rating and

reporting data at a fine-grained level (i.e., we may have multiple ratings and reports for each node/type/week tuple). For node/type/week tuples without observed ratings, we aggregate the reporting data at the Census tract level. See the appendix data section for details.

Model

Approach overview: Our model is summarized in Figure 1. The goals are (i) to estimate the true latent state of a particular incident type at a particular location – e.g., what is the true street condition in a particular neighborhood?; and (ii) to quantify biases in the observed reporting data – e.g., which neighborhoods systematically underreport incidents and how do reporting behaviors correlate with demographics? In many urban settings, models are fit using only the frequently observed reporting data, resulting in biased predictions (Xu et al. 2017; Casey, Wilson, and Yokum 2018; Li et al. 2020; Hacker et al. 2022). In contrast, our approach estimates the true latent state using both the frequently observed biased reporting data and the sparsely observed unbiased rating data.

Notation: Consider a network G with n nodes and adjacency matrix E . Nodes are indexed by i and represent neighborhoods, and edges connect adjacent neighborhoods. Each node i has features $X_i \in \mathbb{R}^D$, where D is the number of features. These features include demographic factors that may influence reporting rates. There are τ incident types indexed by k (e.g., rodents, floods, etc.). We index time by week t . The model uses two types of data: sparsely observed unbiased true state measures (e.g., *inspection ratings*) and frequently observed biased data (e.g., *crowdsourced reports*).

Observed data: For some node/type/week tuples, we observe inspection ratings $r_{ikt} \in \mathbb{R}$. These ratings are unbiased observations of the true latent state, but they are only available for a subset of nodes, types, and weeks. We also observe indicators of reports of incidents $T_{ikt} \in \{0, 1\}$, where $T_{ikt} = 1$ indicates that an incident of type k was reported for node i at week t . Reports are obtained from residents and are thus potentially biased proxies of the true latent state, with bias correlating with resident demographics. As discussed in the data section, for some types, both inspection ratings and reports are available at the *sub-node* (granular) level.

We provide the sub-node level notation of our model in the appendix model section.

Model: The *true* inspection rating r_{ikt} captures the condition of incident type k in node i during week t . More formally, the true ratings are drawn from some distribution f_r as a function of the node, type, and week, as follows:

$$\text{True inspection rating: } r_{ikt} \sim f_r(\cdot | i, k, t). \quad (1)$$

We now discuss how we *model* ratings and the probability of observing a report. To model ratings, we learn a *node embedding* and a *type embedding*. Node i 's embedding $e_n[i] \in \mathbb{R}^{E_n}$, where E_n is the embedding dimension, is a low-dimensional representation of a node and captures the node's attributes and position. The node embeddings are learned using a graph neural network (GNN)

(Kipf and Welling 2017; Veličković et al. 2018), which is a deep learning model that leverages graph-structured data by iteratively aggregating and transforming features from neighboring nodes. Thus our node embeddings are *spatially correlated*, capturing the correlation of true incident occurrence across neighborhoods. We also learn type k 's embedding $e_\tau[k] \in \mathbb{R}^{E_\tau}$, where E_τ is the embedding dimension. The type embedding is a low-dimensional representation of a type and captures the type's features, similarity to other types, and relationship to nodes in the graph. Thus our type embeddings capture correlations across types.

We model ratings as follows:

$$\text{Pred. rating: } \hat{r}_{ikt} = e_n[i]^\top e_\tau[k] \quad (2)$$

In words, the predicted rating \hat{r}_{ikt} is estimated as the dot product of node i 's embedding $e_n[i]$ and type k 's embedding $e_\tau[k]$.

We model the probability of observing a report as a type-specific function of demographics and the inspection rating. We learn type-specific reporting parameters to account for the fact that different incident types have different reporting characteristics, a claim we confirm on our real rating data. We model the predicted probability of observing a report $\hat{P}(T_{ikt})$ as the following logistic (σ) function:

$$\text{Pred. prob. of report: } \hat{P}(T_{ikt}) = \sigma(\alpha^* r_{ikt}^* + \theta^{*\top} X_i). \quad (3)$$

As we discuss further below, the values used for r_{ikt}^* , α^* , θ^* depend on whether a rating r_{ikt} is observed in node/type/week tuple (i, k, t) and whether ratings for other nodes i' for type k are observed ($r_{i'kt}$). We must consider these cases separately because we cannot simultaneously learn the rating r_{ikt} and the type-specific reporting coefficients $[\alpha_k, \theta_k]$ —there is a fundamental unidentifiability between whether conditions are bad (low rating r_{ikt}) but the area does not make a report (small reporting coefficients $[\alpha_k, \theta_k]$) or conditions are good (high rating r_{ikt}) and no report is needed. We now describe the three different cases:

Case 1 – A rating r_{ikt} is observed: Here, the probability of observing a report is a function of demographics X_i and the true observed rating, so we set $r_{ikt}^* = r_{ikt}$. We estimate type specific reporting coefficients, so $[\alpha_k^*, \theta_k^*] = [\alpha_k, \theta_k]$.

Case 2 – No rating r_{ikt} is observed at node i but ratings $r_{i'kt}$ for type k are observed at other nodes i' : Here, we do not have access to node i 's true rating, so we model the probability of observing a report as a function of demographics X_i and the predicted ratings, so we set $r_{ikt}^* = \hat{r}_{ikt}$. We use type specific reporting coefficients, so $[\alpha_k^*, \theta_k^*] = [\alpha_k, \theta_k]$, which are learned via nodes i' for which ratings $r_{i'kt}$ are observed.

Case 3 – No ratings r_{ikt} for type k are observed at any node: We do not observe the true rating, so we model the probability of observing a report as a function of demographics X_i and the *predicted ratings*, so we set $r_{ikt}^* = \hat{r}_{ikt}$. We cannot simultaneously learn the rating r_{ikt} and type-specific reporting coefficients $[\alpha_k, \theta_k]$. Thus, we borrow information from types with observed ratings and use the mean reporting coefficients across these types, so $[\alpha_k^*, \theta_k^*] = [\bar{\alpha}, \bar{\theta}]$.

For observed types k , we can recover type-specific reporting coefficients $[\alpha_k, \theta_k]$ to account for different types’ likelihoods of being reported when incidents occur. For instance, residents may be more likely to report rodents than a noise complaint. We then implicitly assume that the mean coefficients $[\bar{\alpha}, \bar{\theta}]$ are reasonable for types with unobserved ratings, i.e., the reporting coefficients transfer across types to some extent.

We note that our approach extends to other parameterizations of r_{ikt} and T_{ikt} . For example, while our described model predicts constant ratings \hat{r}_{ikt} and reporting probabilities $\hat{P}(T_{ikt})$ over time, our method generalizes to spatiotemporal GNN-based models. Full details on our model are provided in the appendix model section.

Loss function: To calculate our loss function we first separately evaluate our model’s performance in predicting reports and ratings. Our final loss is a weighted sum of each of these individual loss components. More formally, the loss function consists of four parts:

(i) *Report loss for data points with unobserved ratings:* Binary cross entropy (BCE) loss between the true report status T_{ikt} and the predicted probability of a report $\hat{P}(T_{ikt})$ for data points with unobserved ratings.

$$\mathcal{L}_{\text{unobs}} = \sum_{ikt} \mathbb{1}(r_{ikt} \text{ unobserved}) \cdot \text{BCE}(\hat{P}(T_{ikt}), T_{ikt}) \quad (4)$$

(ii) *Report loss for data points with observed ratings:* BCE between the true report status T_{ikt} and the predicted probability of a report $\hat{P}(T_{ikt})$ for fine-grained data points with observed ratings.

$$\mathcal{L}_{\text{obs}} = \sum_{ikt} \mathbb{1}(r_{ikt} \text{ is observed}) \cdot \text{BCE}(\hat{P}(T_{ikt}), T_{ikt}) \quad (5)$$

(iii) *Rating loss:* Mean squared error (MSE) between the true rating r_{ikt} and the predicted rating \hat{r}_{ikt} .

$$\mathcal{L}_{\text{rating}} = \sum_{ikt} \mathbb{1}(r_{ikt} \text{ is observed}) \cdot \text{MSE}(\hat{r}_{ikt}, r_{ikt}) \quad (6)$$

(iv) *Regularization loss:* L^2 norm of the predicted ratings \hat{r}_{ikt} for data points with unobserved ratings. We include this loss to prevent our predicted ratings from growing excessively large.

$$\mathcal{L}_{\text{reg}} = \sum_{ikt} \mathbb{1}(r_{ikt} \text{ is unobserved}) \cdot \hat{r}_{ikt}^2 \quad (7)$$

The overall loss is as follows:

$$\mathcal{L} = \mathcal{L}_{\text{unobs}} + \gamma_1 \cdot \mathcal{L}_{\text{obs}} + \gamma_2 \cdot \mathcal{L}_{\text{rating}} + \gamma_3 \cdot \mathcal{L}_{\text{reg}} \quad (8)$$

We use weights $\gamma_1, \gamma_2, \gamma_3$ and fix the weight on $\mathcal{L}_{\text{unobs}}$ to 1. We select weights via a hyperparameter search minimizing the RMSE of predicted reports and ratings on an unseen validation split. To aid model estimation in real data settings, especially when ratings are sparsely observed, we add two additional losses. Full details are in the appendix model section.

Semi-synthetic experiments

We now validate our approach on semi-synthetic data, using real crowdsourced data but synthetic ratings. In this setting, our model is *well-specified* and captures the true relationship between ratings and reports. An advantage of our synthetic data is that we can know and vary the synthetic parameters. Using this data, we verify that under well-specified conditions our model can (i) better predict ground-truth ratings compared to using either the ratings or reports datasets alone and (ii) recover the reporting parameters.

Experimental setup

For our semi-synthetic experiments, we use real reporting data T_{ikt} as described in the data section, and we use demographic data X_i from the U.S Census Bureau (United States Census Bureau 2024a,b,c,d,e,f). We generate synthetic inspection ratings r_{ikt} by inverting eq. (3):

$$r_{ikt} = \frac{1}{\alpha_k} (\text{logit}(\mathbb{E}_t(T_{ikt})) - \theta_k^\top X_i). \quad (9)$$

Here, $\mathbb{E}_t(T_{ikt})$ is defined as the empirical frequency of T_{ikt} over all weeks in the dataset and $[\alpha_k, \theta_k]$ are type-specific reporting coefficients. Our synthetically generated inspection ratings r_{ikt} aim to distributionally match our real inspection ratings described in the data section. To match the sparsity pattern, we generate a synthetic version of each inspection rating available in the real data (matching time and fine-grained location). To test the limits of our model with sparse data, we also run experiments where we further subsample inspection ratings in the training set. To reflect real-world reporting parameters, for each type k , we draw all reporting parameters θ_k (except for the intercept and α_k) from a Gaussian with a standard deviation of 0.1 and a mean equal to the average reporting coefficients predicted by a logistic regression model run on the real inspection rating data.² Full details on our synthetic inspection ratings are available in the appendix semi-synthetic data section.

We report results averaged across 20 trials. For each trial, we draw a set of reporting coefficients $[\alpha_k, \theta_k]$; generate a new set of synthetic ratings; refit the model to that dataset; and evaluate the predicted ratings, reports, and reporting coefficients. We use a time-based split. We train on data from January 2022 to June 2023 and test on data from July 2023 to December 2023. We wish to assess the effect of using reports and ratings. Thus, we compare predictions and reporting parameter inferences from models with (i) both reports and ratings (*full model*), (ii) only reports (*reports-only model*), and (iii) only ratings (*ratings-only model*).

To evaluate the models, we compare the model predictions (of future reports and ratings) with test time ground truth reports and ratings. Our primary evaluation metric is the correlation between our model’s predicted ratings/probabilities of a report and the average true ratings/report statuses. We use this correlation measure because it evaluates

²We set the intercept of θ_k such that our generated r_{ikt} are zero mean. And we set α_k such that our generated r_{ikt} have a standard deviation of 1. Thus, our generated and real inspection ratings take on both negative and nonnegative values.

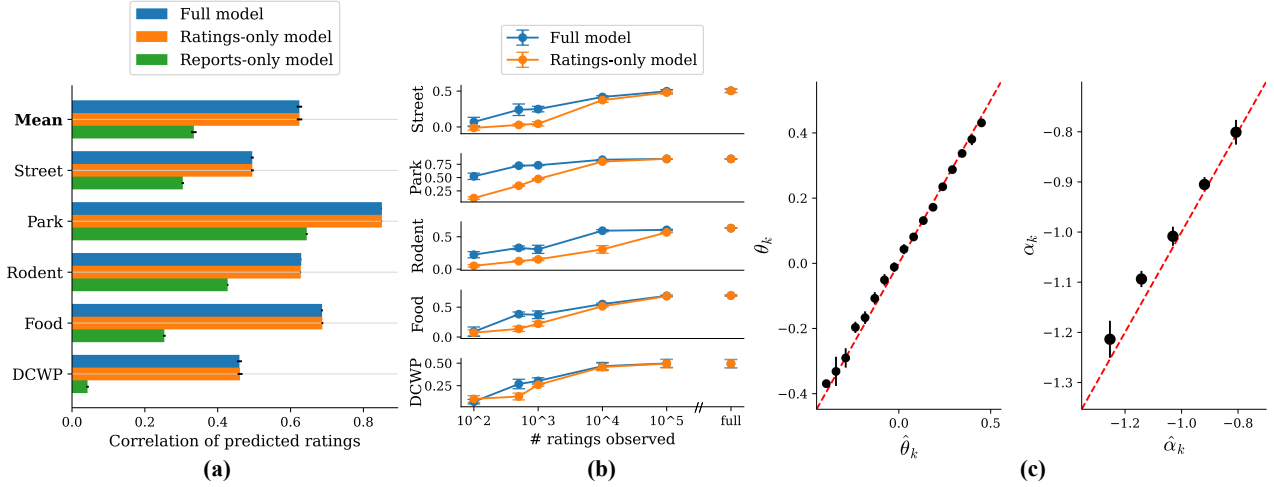


Figure 3: *Semi-synthetic experimental results.* We calculate the correlation between the average predicted and true rating for each node/type pair. We find that (a) our full model predicts ratings that are more correlated with ground truth than a model that uses only reporting data, and (b) as ratings are more sparsely observed, for types where reports are predictive of ratings, our full model predicts ratings that are more correlated with ground truth than a model that uses only rating data. (c) Our model’s predicted coefficients $[\hat{\theta}_k, \hat{\alpha}_k]$ match the true coefficients $[\theta_k, \alpha_k]$ for all types with observed inspection ratings. The red line indicates perfect inference. Panels (a) and (c) show results averaged across 20 semi-synthetic datasets. Panel (b) shows results averaged across 5 semi-synthetic datasets.

how well our model ranks the severity of incidents across nodes for each type. Appendix Table 3 provides results using RMSE as a metric, and these results are qualitatively similar.

Semi-synthetic data results

Figure 3 shows our synthetic data results. In (a), we compare our full model’s performance in predicting future ratings to the ratings-only model and the reports-only model. In (a) we show results when the full training data is available, and in (b) we show results when only a subsample of ratings is available, to mimic the setting of sparsity. In (c), we show the recovered reporting coefficients compared to the true coefficients. Average correlation and RMSE results for each model are shown in Appendix Table 3. The appendix semi-synthetic experiments section provides further details on our results and metrics.

The full model outperforms a model that uses only crowdsourced reports: Our model’s predicted ratings and reports correlate with ground truth. As shown in Appendix Table 3, across all types, the average correlation between our full model’s predicted probability of a report $\hat{P}(T_{ikt})$ and the true probability $P(T_{ikt})$ is $r = 0.49$ ($p < 0.001$ for 81% of types). Across all types with observed ratings, the average correlation between our full model’s predicted rating \hat{r}_{ikt} and the true rating r_{ikt} is $r = 0.62$ ($p < 0.001$ for all types). Our full model recovers the empirical average ratings for each node/type pair in the training data ($r = 1.00$) and the remaining error is due to the distribution shift between the train and test time periods.

Compared to the reports-only model, the full model predicts ratings that better correlate with ground truth ($r = 0.62$

for the full model versus 0.33 for the reports-only model). Figure 3 (a) shows the full model’s improvement for each type with observed ratings. The reports-only model’s ratings are poorly correlated with the ground-truth ratings because it *cannot* recover the true reporting coefficients $[\alpha_k, \theta_k]$. In our semi-synthetic data, the reporting probability $P(T_{ikt})$ is defined as a logistic function of demographics X_i and the true rating r_{ikt} , parameterized by reporting coefficients $[\alpha_k, \theta_k]$. The reports-only model observes the true demographic data and can accurately estimate the probability of a report, however since it *does not* observe ground-truth rating data it learns incorrect reporting coefficients $[\alpha_k, \theta_k]$ and ratings.

The full model outperforms a model that only uses inspection rating data when rating data is sparse: Next we compare our full model’s predicted ratings to the ratings-only model’s predictions. We show that the full model is especially valuable when ratings are expensive to obtain and are sparsely observed. We run experiments with artificially sparsified ratings by subsampling ratings for each type with observed ratings. We plot the results in Figure 3 (b). For types where reports are predictive of ratings, as we decrease the number of ground-truth ratings that the model observes, our full model’s predicted ratings remain correlated with the true ratings, while the ratings-only model approaches random prediction ($r = 0$). In particular, when reports are predictive of ratings (reports-only model achieves a high correlation) the full model obtains higher correlations on subsampled data (e.g., for park and rodent types). This is because in these cases the full model can use reporting data to augment the sparse ratings and improve rating predictions. More details on the subsampled experiments are provided in the appendix model section.

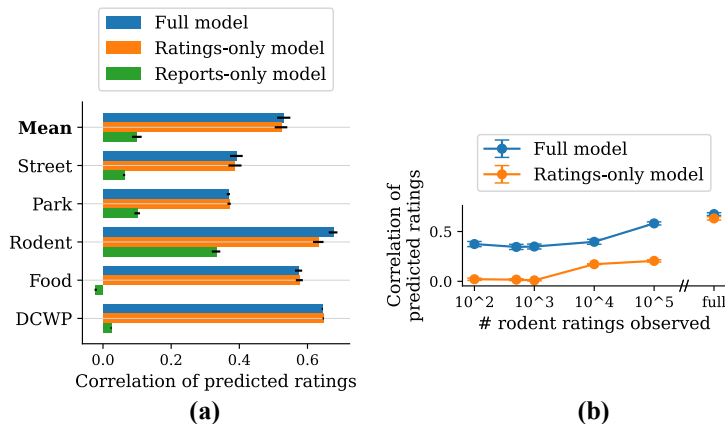


Figure 4: *Real data experimental results.* We calculate the correlation between the average predicted and true rating for each node/type pair. We find that (a) our full model predicts ratings that are more correlated with ground truth than a model that uses only reporting data, and (b) as ratings are more sparsely observed, for types where reports are predictive of ratings, our full model predicts ratings that are more correlated with ground truth than a model that uses only rating data. We plot the mean correlation and 95% CIs over all contiguous two-year periods between 2021 and 2023.

The model recovers the true reporting coefficients: As shown in Figure 3 (c), our model recovers the true reporting coefficients $[\alpha_k, \theta_k]$ for incident types with observed ratings. This can only be done by using both types of data together – one cannot identify both the reporting coefficients $[\alpha_k, \theta_k]$ and the inspection ratings r_{ikt} using *only* crowdsourced reporting data or *only* rating data. In particular, with only crowdsourced reporting data it is impossible to distinguish between a bad inspection rating that is never reported and a truly good inspection rating. Thus, to identify reporting coefficients, one must either use *both* rating and reporting data or make strong parametric assumptions (e.g., assume a shared reporting model across types). Additionally, our model only estimates type-specific reporting coefficients for incident types with observed ratings. For incident types without observed ratings, we use the average reporting coefficients learned across incident types with observed ratings. Thus our model can only estimate the true reporting coefficients for types with observed ratings and we accordingly evaluate its performance on these types.

The model can learn across types in well-specified settings: In Appendix Table 4 we show that, compared to the reports-only model, our full model predicts ratings that are more correlated with ground truth even for types with fully unobserved ratings. This shows that ground-truth rating data for *observed* types can be beneficial in predicting ratings for *unobserved* types. Importantly, this demonstrates that our model can learn ground-truth characteristics that generalize *across* types, in settings where reporting behavior across types is related. We note that the ratings-only model can only learn ratings for types with observed ratings. Thus, it cannot make rating predictions for types with unobserved ratings.

Overall, our semi-synthetic results show that our approach helps if our model is well-specified. In the next section, we assess our approach on real data.

Real-world case study: New York City crowdsourced reporting

We now evaluate our approach using real world data, both in terms of predicting future ground-truth ratings and in recovering reporting biases as they correlate with demographics.

Experimental setup

We use real reporting data T_{ikt} and rating data r_{ikt} , as described in the data section. As in the semi-synthetic experiments, we use demographic data X_i from the U.S Census Bureau (United States Census Bureau 2024a,b,c,d,e,f). When a government inspection occurs, we assume that the resulting rating remains constant over time until the next inspection occurs. We split our data into a train and test set using a time-based split, as is standard in urban prediction tasks (Yu, Yin, and Zhu 2018; Farahmand, Xu, and Mostafavi 2023; Huang et al. 2023; Agostini, Pierson, and Garg 2024). We create splits over every contiguous two-year period between January 2021 and December 2023 (13 total periods). For each two year time period, we train on the first 18 months of data and test on the last 6 months. We report results averaged across all 13 time splits.³

Results

Prediction in our real data setting is more challenging than in our semi-synthetic setting due to model misspecification. For example, we model the probability of a report as a logistic function of demographics and true ratings, which allows us to quantify how reporting rates vary by demographics. But in reality, it is likely that reports are generated by

³For all real data experiments, we report CIs over the 13 two-year time splits between January 2021 and December 2023. We note that this means that the CIs are calculated across overlapping datasets.

a more complex function with more complex inputs. Nevertheless, our model’s predicted ratings and reports still correlate with ground truth. Across all types, the average correlation between our full model’s predicted probability of a report $\hat{P}(T_{ikt})$ and the true probability of a report $P(T_{ikt})$ is $r = 0.24$ ($p < 0.001$ for 83% of types). As shown in Appendix Table 3, across all types with observed inspection ratings, the average correlation between our full model’s predicted rating \hat{r}_{ikt} and the true rating r_{ikt} is $r = 0.53$ ($p < 0.001$ for all types). We also report RMSE results in Appendix Table 3.

Compared to the reports-only model, our full model’s predicted ratings are more correlated with ground truth:

The correlation between the full model’s predicted ratings and the ground-truth ratings is $r = 0.53$ versus 0.10 for the reports-only model. Figure 4 (a) shows the full model’s improvement in predicting ratings for each type with observed ratings. Compared to the reports-only model, the full model’s predicted probabilities of reports are less correlated with ground truth reports ($r = 0.24$ for the full model versus 0.54 for the reports-only model) because the reports-only model can perfectly fit to the biased reporting data, while the full model primarily aims to learn inspection ratings. We find in both semi-synthetic and real data, that compared to a model that uses reporting data alone, our full model’s predicted ratings are more correlated with ground truth. This highlights a key contribution of our model which leverages sparse unbiased rating data over prior work which only learns from biased reporting data.

The full model outperforms a model that only uses inspection rating data when rating data is sparse and reports are predictive of ratings:

Next we compare our full model’s predicted ratings to the ratings-only model’s predictions. We show that the full model is especially valuable when (i) ratings are expensive to obtain and are sparsely observed and (ii) reports are predictive of ratings. Similar to the semi-synthetic setting, we run experiments with artificially sparsified ratings by subsampling ratings for types with observed ratings. We plot the results in Figure 4 (b). For the rodent type, where reports are predictive of ratings, as we decrease the number of ground-truth ratings that the model observes, our full model’s predicted ratings remain correlated with the true ratings, while the ratings-only model approaches random prediction ($r = 0$). For the other four incident types with observed ratings, reports are not predictive of ratings (reports-only model achieves a low correlation, $r \leq 0.1$). Thus in these cases the model’s predictive power comes mostly from rating data, and reporting data provides minimal benefit in improving rating predictions. More details on the subsampled experiments are provided in the appendix model section.

The model learns demographic predictors of underreporting:

θ_k measures the contribution of each demographic feature in X_i to the reporting rate. We estimate θ_k by fitting univariate variants of our full model. Each univariate model is trained on both rating and reporting data but only uses one demographic feature. We run a separate univariate

Covariate	Mean coefficient
log(Population density)	0.250 ± 0.058
log(Median income)	0.173 ± 0.020
Bachelors degree population	0.159 ± 0.018
Households occupied by renter	0.115 ± 0.029
Median age	0.104 ± 0.016
White population	0.093 ± 0.012
True inspection rating	-0.197 ± 0.009

Table 1: *Univariate demographic coefficients.* We report the average predicted univariate demographic coefficients across types with observed ratings. The estimated coefficients capture known demographic factors: tracts that are more dense, have a higher income, are more educated, are older, or have more white residents are more likely to report incidents. We also report the average coefficient on the true inspection rating across all univariate models. Tracts that have worse ratings are more likely to have reports. We report the mean coefficients and 95% CIs over all contiguous two year periods between 2021 and 2023.

model for each demographic feature in X_i . Table 1 shows that the inferred coefficients capture known demographic predictors of underreporting. We find that conditional on ground-truth, neighborhoods with higher population density, higher median income, higher proportion of the population with a bachelor’s degree, older residents, higher proportion of white residents, and worse ground-truth states all report incidents at higher rates; these estimates are consistent with those of other work (Kontokosta and Hong 2021; Agostini, Pierson, and Garg 2024; Liu, Bhandaram, and Garg 2024; Franchi et al. 2025), and add further evidence of demographic bias in crowdsourced reporting, across incident types. Coefficients estimated by a multivariate model are in Appendix Table 5.

Our full model’s predicted ratings are spatially correlated and capture correlations across incident types:

We evaluate the interpretability of our model’s predicted ratings by analyzing how well they correlate across nodes and types. We first analyze the predicted ratings’ spatial correlation. For each node i , we create a vector $\mathbf{r}_i = \{r_{ikt}\}_{k=1}^7$ of predicted ratings over all types k . We use each node’s \mathbf{r}_i vector to cluster the nodes into 4 groups. We find that the predicted clusters are spatially correlated and demographically distinct. Figure 5 shows that our clusters are spatially correlated, e.g., there is a clear spatial separation. The clusters correlate with New York City (NYC) borough lines, e.g., Manhattan falls mostly into cluster 1 and the Bronx falls mostly into cluster 2. There are substantial socioeconomic and other demographic differences between Boroughs; the full model also captures intra-Borough differences, such as that between Midtown Manhattan and Harlem. We similarly find significant demographic differences between each cluster, and we report the statistically significant differences in Appendix Table 6.

We compare our full model clustering to the ratings-only model clustering. Figure 5 shows that our full model learns more spatially correlated ratings than the ratings-only model. The higher spatial correlations from our full model

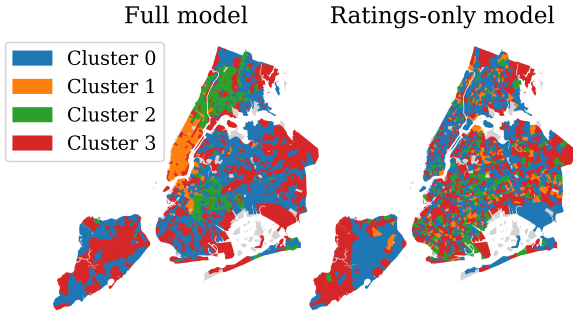


Figure 5: *Our full model learns spatially correlated ratings.* Using each node’s vector of learned ratings over types, we cluster nodes into 5 groups using a k means clustering algorithm. Our model, which learns from both reports and ratings, predicts more spatially clustered ratings than a model which learns only from ratings.

as compared to the ratings-only model are consistent with prior work (Agostini, Pierson, and Garg 2024) and potentially render our full model more interpretable.

Next, we analyze our predicted ratings’ across complaint types. For each type k , we create a vector $\mathbf{r}_k = \{r_{ikt}\}_{i=1}^n$ of predicted ratings over all nodes i to cluster the types into 8 groups. We find that each group contains a coherent cluster of types, and in Appendix Table 7 we describe and list the types captured by each cluster. Additionally, Appendix Figure 6 shows that the dimension of highest variability (i.e., first PCA dimension) of the \mathbf{r}_k vectors captures type frequency (i.e., $\mathbb{E}_{it}[T_{ikt}]$). These results show that our full model’s predicted ratings emulate ground truth ratings since both are spatially correlated and capture similarities across incident types.

Discussion

We address the challenging problem of estimating graph neural networks (GNNs) in settings where we observe biased outcome data. In these settings, nodes have a true latent state that is sparsely observed (e.g., via government inspection ratings). We also frequently observe biased proxies of the latent states (e.g., via crowdsourced reports). We propose a GNN-based model that uses frequently observed biased reporting data and sparsely observed unbiased rating data. We apply our model to New York City 311 data and show that (i) our model makes better predictions of the ground-truth latent state compared to both a baseline model trained only on reporting data and a baseline model trained only on rating data, especially when rating data is sparsely observed; (ii) our model’s inferred reporting coefficients capture known demographic factors associated with underreporting; and (iii) our model’s learned ratings are interpretable and capture correlation between nodes and 311 complaint types, as evidenced by the fact that ratings cluster spatially over nodes and thematically over types.

Our approach contributes to advancing efficiency and fairness in urban resource allocation. Explicitly modeling the demographic factors that influence reporting behaviors may

help city officials identify and address service gaps in communities that would otherwise remain hidden due to underreporting biases. Identifying service gaps enables more targeted civic engagement strategies, more equitable distribution of limited resources, and decision support systems that allow urban planners to simulate how addressing reporting biases might lead to more just outcomes across diverse neighborhoods.

Our data and model open several avenues for additional applications and future work. Our dataset serves as an ideal setting in which to study distribution shifts over time. Our model provides a particular example of how to estimate reporting propensity; one line of future work could investigate whether other methods of incorporating reporting data could produce more accurate rating predictions. Another natural direction is to apply our model to other urban settings with biased reporting data, such as crime reporting or public health incident tracking, where similar demographic reporting disparities likely exist. As discussed in this paper, reporting biases often correlate with demographics, so learning only from reporting data risks introducing bias against underserved populations – a risk that extends to any crowdsourced urban data collection mechanism. Beyond urban applications, other GNN tasks, such as environmental monitoring and epidemic forecasting, may also have sparsely observed ground truth and frequently observed biased proxies, suggesting our methodology could serve as an approach for responsible machine learning across numerous domains where equitable resource allocation depends on accurate understanding of underlying conditions rather than reporting patterns.

Acknowledgments

The authors thank Vince Bartle, Serina Chang, Erica Chiang, Matt Franchi, Sophie Greenwood, Raj Movva, and Kenny Peng for helpful conversations. SB is supported by NSF GRFP Grant DGE #2139899. SS is supported by NSF GRFP Grant DGE #2141064 and the Hertz Fellowship. EP is supported by a Google Research Scholar award, an AI2050 Early Career Fellowship, NSF CAREER #2142419, a CIFAR Azrieli Global scholarship, a gift to the LinkedIn-Cornell Bowers CIS Strategic Partnership, the Survival and Flourishing Fund, Open Philanthropy, and the Abby Joseph Cohen Faculty Fund. NG is supported by NSF CAREER IIS-2339427, and Cornell Tech Urban Tech Hub, Meta, and Amazon research awards. Any opinions, findings, conclusions, or recommendations expressed in this material are those of the authors and do not necessarily reflect the views of the funders.

References

- Agonafir, C.; Pabon, A. R.; Lakhankar, T.; Khanbilvardi, R.; and Devineni, N. 2022. Understanding New York City street flooding through 311 complaints. *Journal of Hydrology*, 605: 127300.
- Agostini, G.; Pierson, E.; and Garg, N. 2024. A Bayesian spatial model to correct under-reporting in urban crowd-

- sourcing. In *Proceedings of the AAAI Conference on Artificial Intelligence*, volume 38, 21888–21896.
- Appleby, G.; Liu, L.; and Liu, L.-P. 2020. Kriging convolutional networks. In *Proceedings of the AAAI Conference on Artificial Intelligence*, volume 34, 3187–3194.
- Arazo, E.; Ortego, D.; Albert, P.; O’Connor, N. E.; and McGuinness, K. 2020. Pseudo-labeling and confirmation bias in deep semi-supervised learning. In *2020 International Joint Conference on Neural Networks (IJCNN)*, 1–8. IEEE.
- Bauer, J.; and Aschenbruck, N. 2018. Design and implementation of an agricultural monitoring system for smart farming. In *2018 IoT Vertical and Topical Summit on Agriculture-Tuscany (IOT Tuscany)*, 1–6. IEEE.
- Belkin, M.; Niyogi, P.; and Sindhvani, V. 2006. Manifold regularization: A geometric framework for learning from labeled and unlabeled examples. *Journal of Machine Learning Research*, 7(11).
- Brimos, P.; Karamanou, A.; Kalampokis, E.; Mamalis, M. E.; and Tarabanis, K. 2023. Explainable graph neural networks on linked statistical data for predicting Scottish house prices. In *Proceedings of the 27th Pan-Hellenic Conference on Progress in Computing and Informatics*, 36–41.
- Brody, S.; Alon, U.; and Yahav, E. 2022. How attentive are graph attention networks? In *International Conference on Learning Representations (ICLR)*.
- Budde, M.; De Melo Borges, J.; Tomov, S.; Riedel, T.; and Beigl, M. 2014. Leveraging spatio-temporal clustering for participatory urban infrastructure monitoring. In *Proceedings of the First International Conference on IoT in Urban Space*, 32–37.
- Casey, P. C.; Wilson, K. H.; and Yokum, D. 2018. A cautionary tail: A framework and case study for testing predictive model validity. *arXiv preprint arXiv:1807.03860*.
- Chang, S.; Fournay, A.; and Horvitz, E. 2024. Measuring vaccination coverage and concerns of vaccine holdouts from web search logs. *Nature Communications*, 15(1): 6496.
- Cheng, S.; Lu, F.; Peng, P.; and Wu, S. 2018. A spatiotemporal multi-view-based learning method for short-term traffic forecasting. *ISPRS International Journal of Geo-Information*, 7(6).
- Clark, B. Y.; Brudney, J. L.; Jang, S.-G.; and Davy, B. 2020. Do advanced information technologies produce equitable government responses in coproduction: An examination of 311 systems in 15 US cities. *The American Review of Public Administration*, 50(3): 315–327.
- Cui, H.; Lu, Z.; Li, P.; and Yang, C. 2022. On positional and structural node features for graph neural networks on non-attributed graphs. In *Proceedings of the 31st ACM International Conference on Information & Knowledge Management, CIKM ’22*, 3898–3902. Association for Computing Machinery.
- Dai, E.; Aggarwal, C.; and Wang, S. 2021. NRGNN: Learning a label noise resistant graph neural network on sparsely and noisily labeled graphs. In *Proceedings of the 27th ACM SIGKDD Conference on Knowledge Discovery & Data Mining*, 227–236. Association for Computing Machinery.
- Farahmand, H.; Xu, Y.; and Mostafavi, A. 2023. A spatial-temporal graph deep learning model for urban flood now-casting leveraging heterogeneous community features. *Scientific Reports*, 13(1): 6768.
- Franchi, M.; Garg, N.; Ju, W.; and Pierson, E. 2025. Bayesian modeling of zero-shot classifications for urban flood detection.
- Gao, Q.; Huang, Y.; Zerhouni, E. G.; and Zheng, Y. 2024. How to improve citizen engagement on public service platforms? The impact of government responsiveness.
- Gómez, J. A.; Patiño, J. E.; Duque, J. C.; and Passos, S. 2019. Spatiotemporal modeling of urban growth using machine learning. *Remote Sensing*, 12(1): 109.
- Grover, A.; and Leskovec, J. 2016. node2vec: Scalable feature learning for networks. In *Proceedings of the 22nd ACM SIGKDD International Conference on Knowledge Discovery and Data Mining*, 855–864. Association for Computing Machinery.
- Hacker, K. P.; Greenlee, A. J.; Hill, A. L.; Schneider, D.; and Levy, M. Z. 2022. Spatiotemporal trends in bed bug metrics: New York City. *PloS one*, 17(5): 1–14.
- He, S.; Luo, Q.; Du, R.; Zhao, L.; He, G.; Fu, H.; and Li, H. 2023. STGC-GNNs: A GNN-based traffic prediction framework with a spatial-temporal Granger causality graph. *Physica A: Statistical Mechanics and its Applications*, 623: 128913.
- Hu, T.; Zhu, X.; Duan, L.; and Guo, W. 2018. Urban crime prediction based on spatio-temporal Bayesian model. *PloS one*, 13(10): e0206215.
- Huang, S.; Poursafaei, F.; Danovitch, J.; Fey, M.; Hu, W.; Rossi, E.; Leskovec, J.; Bronstein, M.; Rabusseau, G.; and Rabbany, R. 2023. Temporal graph benchmark for machine learning on temporal graphs. In *Advances in Neural Information Processing Systems*, volume 36, 2056–2073.
- Jiménez-Jiménez, S. I.; Ojeda-Bustamante, W.; Ontiveros-Capurata, R. E.; and Marcial-Pablo, M. d. J. 2020. Rapid urban flood damage assessment using high resolution remote sensing data and an object-based approach. *Geomatics, Natural Hazards and Risk*, 11(1): 906–927.
- Kapoor, A.; Ben, X.; Liu, L.; Perozzi, B.; Barnes, M.; Blais, M.; and O’Banion, S. 2020. Examining COVID-19 forecasting using spatio-temporal graph neural networks. *MLG workshop @ KDD’2020, epiDAMIK workshop @ KDD’2020*.
- Kipf, T. N.; and Welling, M. 2017. Semi-supervised classification with graph convolutional networks. In *International Conference on Learning Representations (ICLR)*.
- Klemmer, K.; Safir, N. S.; and Neill, D. B. 2023. Positional encoder graph neural networks for geographic data. In *International Conference on Artificial Intelligence and Statistics*, 1379–1389. PMLR.
- Kontokosta, C.; Hong, B.; and Korsberg, K. 2017. Equity in 311 reporting: Understanding socio-spatial differentials in the propensity to complain. *arXiv preprint arXiv:1710.02452*.

- Kontokosta, C. E.; and Hong, B. 2021. Bias in smart city governance: How socio-spatial disparities in 311 complaint behavior impact the fairness of data-driven decisions. *Sustainable Cities and Society*, 64: 102503.
- Kyono, T.; Zhang, Y.; and van der Schaar, M. 2020. CASTLE: Regularization via auxiliary causal graph discovery. In *Advances in Neural Information Processing Systems*, volume 33, 1501–1512.
- Li, J.; Xiong, C.; and Hoi, S. C. 2021. CoMatch: Semi-supervised learning with contrastive graph regularization. In *Proceedings of the IEEE/CVF International Conference on Computer Vision*, 9475–9484.
- Li, Y.; Hyder, A.; Southerland, L. T.; Hammond, G.; Porr, A.; and Miller, H. J. 2020. 311 service requests as indicators of neighborhood distress and opioid use disorder. *Scientific Reports*, 10(1): 19579.
- Li, Y.; Yin, J.; and Chen, L. 2023. Informative pseudo-labeling for graph neural networks with few labels. *Data Mining and Knowledge Discovery*, 37(1): 228–254.
- Liu, Z.; Bhandaram, U.; and Garg, N. 2024. Quantifying spatial under-reporting disparities in resident crowdsourcing. *Nature Computational Science*, 4(1): 57–65.
- Liu, Z.; and Garg, N. 2024. Redesigning Service Level Agreements: Equity and Efficiency in City Government Operations. In *Proceedings of the 25th ACM Conference on Economics and Computation*, 309–309.
- Lum, K.; and Isaac, W. 2016. To predict and serve? *Significance*, 13(5): 14–19.
- Mauerman, M.; Tellman, E.; Lall, U.; Tedesco, M.; Colosio, P.; Thomas, M.; Osgood, D.; and Bhuyan, A. 2022. *High-quality historical flood data reconstruction in Bangladesh using hidden Markov models*, 191–210. ISBN 978-3-030-95721-6.
- Mosavi, A.; Ozturk, P.; and Chau, K.-w. 2018. Flood prediction using machine learning models: Literature review. *Water*, 10(11).
- NYC Open Data. 2023. Street Rating.
- NYC Open Data. 2024a. 311 Service Requests from 2010 to Present.
- NYC Open Data. 2024b. Department of Consumer and Worker Protection (DCWP) Inspections.
- NYC Open Data. 2024c. DOHMH New York City Restaurant Inspection Results.
- NYC Open Data. 2024d. Parks Inspection Program – Inspections.
- NYC Open Data. 2024e. Rodent Inspection.
- O’Brien, D. T.; Offenhuber, D.; Baldwin-Philippi, J.; Sands, M.; and Gordon, E. 2017. Uncharted territoriality in coproduction: The motivations for 311 reporting. *Journal of Public Administration Research and Theory*, 27(2): 320–335.
- O’Brien, D. T.; Sampson, R. J.; and Winship, C. 2015. Econometrics in the age of big data: Measuring and assessing “broken windows” using large-scale administrative records. *Sociological Methodology*, 45(1): 101–147.
- Pan, Z.; Wang, Z.; Wang, W.; Yu, Y.; Zhang, J.; and Zheng, Y. 2019. Matrix factorization for spatio-temporal neural networks with applications to urban flow prediction. In *Proceedings of the 28th ACM International Conference on Information and Knowledge Management, CIKM ’19*, 2683–2691. Association for Computing Machinery.
- Peng, F.; Lu, W.; Tan, W.; Qi, K.; Zhang, X.; and Zhu, Q. 2022. Multi-output network combining GNN and CNN for remote sensing scene classification. *Remote Sensing*, 14(6).
- Perozzi, B.; Al-Rfou, R.; and Skiena, S. 2014. DeepWalk: Online learning of social representations. In *Proceedings of the 20th ACM SIGKDD International Conference on Knowledge Discovery and Data Mining*, 701–710. Association for Computing Machinery.
- Pineda, J.; Midtvedt, B.; Bachimanchi, H.; Noé, S.; Midtvedt, D.; Volpe, G.; and Manzo, C. 2023. Geometric deep learning reveals the spatiotemporal features of microscopic motion. *Nature Machine Intelligence*, 5(1): 71–82.
- Qian, S.; Ying, H.; Hu, R.; Zhou, J.; Chen, J.; Chen, D. Z.; and Wu, J. 2023. Robust training of graph neural networks via noise governance. In *Proceedings of the Sixteenth ACM International Conference on Web Search and Data Mining*, 607–615.
- Roy, A.; Roy, K. K.; Ahsan Ali, A.; Amin, M. A.; and Rahman, A. M. 2021. SST-GNN: Simplified spatio-temporal traffic forecasting model using graph neural network. In *Pacific-Asia Conference on Knowledge Discovery and Data Mining*, 90–102. Springer.
- Samal, K. K. R.; Babu, K. S.; and Das, S. K. 2022. Multi-output spatio-temporal air pollution forecasting using neural network approach. *Applied Soft Computing*, 126: 109316.
- Sarto, S. D.; Ranalli, M. G.; Bakar, K. S.; Cappelletti, D.; Moroni, B.; Crocchianti, S.; Castellini, S.; Spataro, F.; Esposito, G.; Ianniello, A.; et al. 2016. Bayesian spatiotemporal modeling of urban air pollution dynamics. In *Topics on Methodological and Applied Statistical Inference*, 95–103.
- Shao, Z.; Xu, Y.; Wei, W.; Wang, F.; Zhang, Z.; and Zhu, F. 2023. Heterogeneous graph neural network with multi-view representation learning. *IEEE Transactions on Knowledge and Data Engineering*, 35(11): 11476–11488.
- Sharma, D.; and Jones, M. 2023. Efficiently learning the graph for semi-supervised learning. In *Proceedings of the Thirty-Ninth Conference on Uncertainty in Artificial Intelligence*, volume 216 of *Proceedings of Machine Learning Research*, 1900–1910.
- Song, Z.; Yang, X.; Xu, Z.; and King, I. 2023. Graph-based semi-supervised learning: A comprehensive review. *IEEE Transactions on Neural Networks and Learning Systems*, 34(11): 8174–8194.
- Sui, Y.; Wang, X.; Wu, J.; Lin, M.; He, X.; and Chua, T.-S. 2022. Causal attention for interpretable and generalizable graph classification. In *Proceedings of the 28th ACM SIGKDD Conference on Knowledge Discovery and Data Mining*, 1696–1705. Association for Computing Machinery.
- Tang, J.; Qu, M.; Wang, M.; Zhang, M.; Yan, J.; and Mei, Q. 2015. LINE: Large-scale information network embed-

- ding. In *Proceedings of the 24th International Conference on World Wide Web*, 1067–1077.
- Tomy, A.; Razzanelli, M.; Di Lauro, F.; Rus, D.; and Della Santina, C. 2022. Estimating the state of epidemics spreading with graph neural networks. *Nonlinear Dynamics*, 109(1): 249–263.
- United States Census Bureau. 2024a. Educational attainment for the population 25 years and over.
- United States Census Bureau. 2024b. Hispanic or latino, and not hispanic or latino by race.
- United States Census Bureau. 2024c. Income in the past 12 months (in 2023 inflation-adjusted dollars).
- United States Census Bureau. 2024d. Median age by sex.
- United States Census Bureau. 2024e. Tenure.
- United States Census Bureau. 2024f. Total population.
- Veličković, P.; Cucurull, G.; Casanova, A.; Romero, A.; Liò, P.; and Bengio, Y. 2018. Graph attention networks. In *International Conference on Learning Representations (ICLR)*.
- Verma, V.; Qu, M.; Kawaguchi, K.; Lamb, A.; Bengio, Y.; Kannala, J.; and Tang, J. 2021. GraphMix: Improved training of GNNs for semi-supervised learning. In *Proceedings of the AAAI Conference on Artificial Intelligence*, volume 35, 10024–10032.
- Wang, G.; Ying, R.; Huang, J.; and Leskovec, J. 2019. Improving graph attention networks with large margin-based constraints. *arXiv preprint arXiv:1910.11945*.
- Wang, L.; Adiga, A.; Chen, J.; Sadilek, A.; Venkatramanan, S.; and Marathe, M. 2022a. CausalGNN: Causal-based graph neural networks for spatio-temporal epidemic forecasting. In *Proceedings of the AAAI Conference on Artificial Intelligence*, volume 36, 12191–12199.
- Wang, L.; Qian, C.; Kats, P.; Kontokosta, C.; and Sobolevsky, S. 2017. Structure of 311 service requests as a signature of urban location. *PLoS one*, 12(10): e0186314.
- Wang, Y.; Wang, H.; Shen, Y.; Fei, J.; Li, W.; Jin, G.; Wu, L.; Zhao, R.; and Le, X. 2022b. Semi-supervised semantic segmentation using unreliable pseudo-labels. In *Proceedings of the IEEE/CVF Conference on Computer Vision and Pattern Recognition*, 4248–4257.
- Wang, Y.; Zheng, J.; Du, Y.; Huang, C.; and Li, P. 2022c. Traffic-GGNN: Predicting traffic flow via attentional spatio-temporal gated graph neural networks. *IEEE Transactions on Intelligent Transportation Systems*, 23(10): 18423–18432.
- Wu, A. P.; Markovich, T.; Berger, B.; Hammerla, N. Y.; and Singh, R. 2023. Causally-guided regularization of graph attention improves generalizability. *Transactions on Machine Learning Research*.
- Wu, L.; Hou, Z.; Yuan, J.; Rong, Y.; and Huang, W. 2024. Equivariant spatio-temporal attentive graph networks to simulate physical dynamics. In *Advances in Neural Information Processing Systems*, volume 36.
- Wu, Y.; Zhuang, D.; Labbe, A.; and Sun, L. 2021. Inductive graph neural networks for spatiotemporal kriging. In *Proceedings of the AAAI Conference on Artificial Intelligence*, volume 35, 4478–4485.
- Xie, Z.; Lv, W.; Huang, S.; Lu, Z.; Du, B.; and Huang, R. 2019. Sequential graph neural network for urban road traffic speed prediction. *IEEE Access*, 8: 63349–63358.
- Xu, L.; Kwan, M.-P.; McLafferty, S.; and Wang, S. 2017. Predicting demand for 311 non-emergency municipal services: An adaptive space-time kernel approach. *Applied Geography*, 89: 133–141.
- Yu, B.; Yin, H.; and Zhu, Z. 2018. Spatio-temporal graph convolutional networks: A deep learning framework for traffic forecasting. In *Proceedings of the 27th International Joint Conference on Artificial Intelligence, IJCAI'18*, 3634–3640. AAAI Press.
- Yu, S.; Xia, F.; Li, S.; Hou, M.; and Sheng, Q. Z. 2023. Spatio-temporal graph learning for epidemic prediction. *ACM Transactions on Intelligent Systems and Technology*, 14(2): 1–25.
- Zamfirescu-Pereira, J.; Chen, J.; Wen, E.; Koenecke, A.; Garg, N.; and Pierson, E. 2022. Trucks don't Mean trump: Diagnosing human error in image analysis. In *Proceedings of the 2022 ACM Conference on Fairness, Accountability, and Transparency*, 799–813.
- Zaouche, M.; and Bode, N. W. 2023. Bayesian spatio-temporal models for mapping urban pedestrian traffic. *Journal of Transport Geography*, 111: 103647.
- Zhan, W.; and Datta, A. 2024. Neural networks for geospatial data. *Journal of the American Statistical Association*, 0: 1–21.
- Zhang, B.; Wang, Y.; Hou, W.; Wu, H.; Wang, J.; Okumura, M.; and Shinozaki, T. 2021. Flexmatch: Boosting semi-supervised learning with curriculum pseudo labeling. In *Advances in Neural Information Processing Systems*, volume 34, 18408–18419.
- Zhou, D.; Bousquet, O.; Lal, T.; Weston, J.; and Schölkopf, B. 2003. Learning with local and global consistency. In *Advances in Neural Information Processing Systems*, volume 16.
- Zhou, X.; Liu, X.; Yu, H.; Wang, J.; Xie, Z.; Jiang, J.; and Ji, X. 2024. Variance-enlarged Poisson learning for graph-based semi-supervised learning with extremely sparse labeled data. In *International Conference on Learning Representations (ICLR)*.
- Zhu, X.; Ghahramani, Z.; and Lafferty, J. D. 2003. Semi-supervised learning using gaussian fields and harmonic functions. In *Proceedings of the 20th International Conference on Machine Learning*, 912–919.

Further details on the data

Details on processing real reporting data: We use reports T_{ikt} from New York City 311 data (NYC Open Data 2024a). We analyze all Census tracts with valid demographic information ($n = 2292$ nodes), complaint types with a reporting frequency greater than 0.1% ($\tau = 139$ types), and all weeks in the three years from 2021 - 2023. $T_{ikt} \in \{0, 1\}$ denotes whether at least one report of type k was made in node i during week t . In total we analyze 9,615,863 reports.

Feature processing: We include demographic features collected for each Census tract. The full list of features that we include is: log population density, percentage of population with a bachelors degree, percentage of households occupied by a renter, log median income, percentage of population that is white, and median age (United States Census Bureau 2024a,b,c,d,e,f). We normalize all features to have mean 0 and standard deviation 1.

Details on processing real rating data: We collect ratings from government inspection data for five complaint types: (i) street conditions (NYC Open Data 2023), (ii) park maintenance or facility conditions (NYC Open Data 2024d), (iii) rodents (NYC Open Data 2024e), (iv) food establishment/mobile food vendor/food poisoning (NYC Open Data 2024c), and (v) DCWP consumer complaints (NYC Open Data 2024b). A summary of the rating data across these five types is provided in Table 2. Each rating is for a fine-grained unit within a Census tract. Street ratings are for street segments; park ratings are for parks; rodent and food ratings are averaged over each Borough-Block-Lot (BBL); and DCWP ratings are averaged over each Census block. We match each fine-grained rating to its corresponding fine-grained report (i.e., reports in that same street segment). For rodents, food, and DCWP the matching is done directly (i.e., we match the aggregated rodent rating for a BBL to the aggregated report for the same BBL). For streets and parks, to account for potential error in the latitude/longitude information for each 311 report, we run a distance heuristic to complete the matching. We match each rating with its nearest report. If the nearest report is above a certain distance threshold, we filter out the rating (consider it unobserved). Within the same tract, all fine-grained ratings and reports are provided to the model and are mapped to the same node’s embedding, as well as the corresponding type’s embedding.

In order for our rating data to represent *unbiased* observations of the true incident states, we must process the data to ensure the inspections are conducted proactively. In particular, we remove inspections triggered by 311 reports. For example, each week DOHMH rodent inspectors run two types of inspections: (i) inspections triggered by 311 reports and (ii) inspections on multiple buildings in a randomly selected set of blocks (NYC Open Data 2024e). Since the data does not indicate what type of inspection was run, we create a heuristic to identify the block by block inspections. Our heuristic selects for inspections that are clustered close together (i.e., in the same block). In particular, we calculate the number of inspections that occur each week in each Census tract, and we keep all inspections that fall in tracts at least at the 50th percentile. Figure 2 shows that our heuristic

picks out the proactively run block by block rodent inspections. We note that the ratings for the other four types we process (street, park, restaurant, and DCWP) are not made in response to reports and thus we do not need to process them further. We also note that while our approach produces ratings that do not present any reporting biases, the ratings could display other biases, e.g. inter-inspector variability (Zamfirescu-Pereira et al. 2022).

Further details on the model

Here we describe our model using notation for the *sub-node* level that some observed ratings and reports are collected at. We also provide additional details about our model and learning procedure.

Notation: We use the same notation as the model section. Nodes are indexed by i and represent neighborhoods. Incident types are indexed by k (e.g., rodents, floods, etc.). We index time by week t . We introduce the following notation: Each node i contains fine-grained geographic units indexed by i^* (e.g. each Census tract contains street segments or buildings).

Observed data: We observe inspection ratings at the sub-node level. Thus, for some fine-grained geographic unit/type/week tuples, we observe ratings $r_{i^*kt} \in \mathbb{R}$. We also observe indicators of reports of incidents. For node/type/week tuples where a ratings is observed, indicators of reports $T_{i^*kt} \in \{0, 1\}$ are also observed at the sub-node level. For node/type/week tuples where *no* rating is observed, indicators of reports $T_{ikt} \in \{0, 1\}$ are observed at the node level.

Model: The *true* inspection rating r_{i^*kt} captures the condition of incident type k in fine-grained unit i^* during week t . More formally, the true ratings are drawn from some distribution f_r as a function of the node, type, and week, as follows:

$$\text{True inspection rating: } r_{i^*kt} \sim f_r(\cdot|i, k, t). \quad (10)$$

We model ratings at the node level using learned node and type embeddings as follows:

$$\text{Predicted rating: } \hat{r}_{ikt} = e_n[i]^\top e_\tau[k]$$

In words, the predicted rating \hat{r}_{ikt} is estimated as the dot product of node i ’s embedding $e_n[i]$ and type k ’s embedding $e_\tau[k]$. Note that our model predicts constant ratings across each fine-grained geographic unit i^* in node i .

We model the probability of observing a report as a type specific logistic function (σ) of the inspection rating and demographics. Since the true inspection ratings are only observed in a subset of node/type/week tuples (i, k, t) , we learn a different reporting model depending on whether a rating r_{i^*kt} is observed in node i and whether ratings in other nodes i' for type k are observed (i.e., whether ratings $r_{i'^*kt}$ are observed). Additionally, since ratings are observed at the sub-node level, for node/type/week tuples (i, k, t) in which ratings are observed, we learn the probability of observing a report at the sub-node level as well (i.e., we learn $P(T_{i^*kt})$). Overall, there are three different cases that we consider.

	Street	Park	Rodent	Food	DCWP
Number of crowdsourced reports	217k	56k	122k	48k	13k
Number of government inspection ratings	91k	18k	238k	30k	9k
Fine-grained collection unit	street segment	park	BBL	BBL	Census block
How are ratings and reports matched?	Matching	Matching	Available in data	Available in data	Available in data

Table 2: *Data summary.* For each of the five incident types for which we process real ratings, we report the total number of reports made between 2021 and 2023, inclusive; the total number of ratings collected between 2021 and 2023, inclusive; what fine-grained unit ratings are collected at (e.g., Borough-Block-Lot or BBL); and whether corresponding ratings and reports were matched by a matching heuristic (each rating was mapped to its nearest report) or whether the matching was available in the data.

*Case 1 – A rating r_{i^*kt} is observed:* In this case, we model the probability of observing a report as a function of the true granular observed rating r_{i^*kt} and demographic features for the corresponding node X_i . We estimate type specific reporting coefficients $[\alpha_k, \theta_k]$. The observed rating is at the sub-node level, and therefore we model the probability of observing a report at the sub-node level as well.

$$\text{Case 1: } \hat{P}(T_{i^*kt}) = \sigma(\alpha_k r_{i^*kt} + \theta_k^\top X_i) \quad (11)$$

*Case 2 – No rating r_{i^*kt} is observed in node i but ratings $r_{i'kt}$ for type k are observed in other nodes i' :* In this case, we do not have access to true ratings in node i , so we model the probability of observing a report as a function of the *predicted rating* \hat{r}_{ikt} and demographic features X_i . We use type specific reporting coefficients $[\alpha_k, \theta_k]$ which are learned via eq. (11) using the nodes i' for which the ground truth ratings $r_{i'kt}$ are observed for type k . The predicted rating is at the node level, and therefore we model the probability of observing a report at the node level as well.

$$\text{Case 2: } \hat{P}(T_{ikt}) = \sigma(\alpha_k \hat{r}_{ikt} + \theta_k^\top X_i) \quad (12)$$

*Case 3 – No rating r_{i^*kt} is observed for type k at any node:* We again do not have access to the true rating, so we model the probability of observing a report as a function of the *predicted rating* \hat{r}_{ikt} and demographic features X_i . We cannot simultaneously learn the rating r_{ikt} and the type specific reporting coefficients $[\alpha_k, \theta_k]$, thus in this case we model the probability of observing a report as a function of the mean reporting coefficients across types with observed ratings $[\bar{\alpha}, \bar{\theta}]$. The predicted rating is at the node level, and therefore we model the probability of observing a report at the node level as well.

$$\text{Case 3: } \hat{P}(T_{ikt}) = \sigma(\bar{\alpha} \hat{r}_{ikt} + \bar{\theta}^\top X_i) \quad (13)$$

Embeddings: We learn node embeddings using a graph neural network (GNN) (Kipf and Welling 2017; Veličković et al. 2018), which is a deep learning model that leverages graph-structured data by iteratively aggregating and transforming feature information from neighboring nodes. The GNN takes in as inputs the graph G and a set of features for each node i . We use one-hot node features which is common in settings like ours without natural node features (Cui et al.

2022). We learn the type embeddings using a linear layer with one-hot type feature inputs.

The details of our model architecture are as follows: We use a 2 layer GNN where each layer consists of a graph convolution, leaky ReLU activation, and batch normalization. We use an intermediate dimension equal to the number of nodes $n = 2292$ and an embedding dimension of $E_n = E_\tau = 50$.

Batching: We batch our data such that data points with observed ratings and unobserved ratings are batched separately. During training, we freeze the reporting model for batches for which there are no observed ratings (i.e., we learn the reporting coefficients only from types for which ratings are observed).

Loss function: We calculate loss on both our predicted ratings and our predicted probabilities of reports. For node-/type/week tuples (i, k, t) with observed ratings, we observe fine-grained rating and reporting data (e.g., for each individual street segment), and thus our model also calculates loss at the fine-grained level.

Our final loss function is a weighted sum of four loss components:

(i) *Report loss for data points with **unobserved** inspection ratings:* Binary cross entropy (BCE) between the true report status T_{ikt} and predicted probability of a report $\hat{P}(T_{ikt})$ for data points with unobserved inspection ratings.

$$\mathcal{L}_{\text{unobs}} = \sum_{ikt} \mathbb{1}(r_{ikt} \text{ is unobserved}) \cdot \text{BCE}(\hat{P}(T_{ikt}), T_{ikt}) \quad (14)$$

(ii) *Report loss for data points with **observed** inspection ratings:* BCE between the true fine-grained report status T_{i^*kt} and the predicted fine-grained probability of a report $\hat{P}(T_{i^*kt})$ for data points with fine-grained observed inspection ratings.

$$\mathcal{L}_{\text{obs}} = \sum_{i^*kt} \mathbb{1}(r_{i^*kt} \text{ is observed}) \cdot \text{BCE}(\hat{P}(T_{i^*kt}), T_{i^*kt}) \quad (15)$$

(iii) *Rating loss:* Mean squared error (MSE) between the true fine-grained rating r_{i^*kt} and the predicted fine-grained rat-

		Full model	Ratings-only model	Reports-only model
Semi-synthetic	Correlation of reports	0.4680 ± 0.0020	–	0.4840 ± 0.0007
	RMSE of reports	0.0774 ± 0.0009	–	0.0586 ± 0.0001
	Correlation of ratings	0.6243 ± 0.0075	0.6246 ± 0.0075	0.3345 ± 0.0077
	RMSE of ratings	1.0358 ± 0.0257	1.0331 ± 0.0262	–
Real data	Correlation of reports	0.2371 ± 0.0110	–	0.5406 ± 0.0063
	RMSE of reports	0.1104 ± 0.0025	–	0.0566 ± 0.0012
	Correlation of ratings	0.5303 ± 0.0194	0.5223 ± 0.0185	0.0993 ± 0.0143
	RMSE of ratings	0.5833 ± 0.0123	0.5852 ± 0.0116	–

Table 3: *Experimental results.* For both semi-synthetic and real data, we compare our full model (which uses both reporting and rating data) to a reports-only and a ratings-only model. Compared to both baselines, our full model can estimate ratings without compromising accuracy in predicting reports. We calculate the correlation and RMSE between our predicted probabilities of reports and the true probabilities for all node/type pairs. We calculate the correlation and RMSE between our predicted ratings and the true ratings for all nodes and for all types with observed ratings. On the semi-synthetic data, we report the mean correlation and 95% CIs across 20 synthetic datasets. On the real data, we report the mean correlation and 95% CIs over all contiguous two year periods between 2021 and 2023.

ing \hat{r}_{i*kt} .

$$\mathcal{L}_{\text{rating}} = \sum_{i*kt} \mathbb{1}(r_{i*kt} \text{ is observed}) \cdot \text{MSE}(\hat{r}_{i*kt}, r_{i*kt}) \quad (16)$$

(iv) *Regularization loss:* L^2 norm of the predicted ratings for data points with unobserved ratings. We include this loss to maintain stable training and prevent our predicted ratings from growing excessively large.

$$\mathcal{L}_{\text{reg}} = \sum_{ikt} \mathbb{1}(r_{ikt} \text{ is unobserved}) \cdot L^2(\hat{r}_{ikt}) \quad (17)$$

The overall loss is as follows:

$$\mathcal{L} = \mathcal{L}_{\text{unobs}} + \gamma_1 \cdot \mathcal{L}_{\text{obs}} + \gamma_2 \cdot \mathcal{L}_{\text{rating}} + \gamma_3 \cdot \mathcal{L}_{\text{reg}} \quad (18)$$

We use weights $\gamma_1, \gamma_2, \gamma_3$ and fix the weight on $\mathcal{L}_{\text{unobs}}$ to 1.

Hyperparameter search: We conduct a hyperparameter search over the loss weights $\gamma_1, \gamma_2, \gamma_3$, embedding dimension sizes, number of layers, batch size, and learning rate using Weights and Biases on a validation set unseen at train or test time. We select the set of hyperparameters that maximize the correlation of predicted reports and ratings. Based on the hyperparameter search, we run experiments with a learning rate of 0.01 and a batch size of 16000. Our full model uses weights $\gamma_1 = 20, \gamma_2 = 1, \gamma_3 = 10^{-6}$. All experiments are conducted on a cluster with access to NVIDIA A100 and A6000 GPUs. Our model can comfortably train on one GPU.

Baseline models: In our experiments, we wish to assess the effect of using reports and ratings. Thus, we compare inferences from models with (i) both reports and ratings (*full model*), (ii) only reports (*reports-only model*), and (iii) only

ratings (*ratings-only model*). The full model uses both reporting and rating data and all demographic coefficients. Its hyperparameters are set to the specifications listed above. The reports-only is mostly identical to the full model, except it sets a weight of 0 on the loss terms that evaluate against ground-truth ratings $\mathcal{L}_{\text{rating}}$. It also learns type specific reporting coefficients $[\theta_k, \alpha_k]$ for all types (not just types with observed ratings) using all datapoints (not just datapoints with observed ratings, since no datapoints have observed ratings!). The ratings-only is mostly identical to the full model, except it sets a weight of 0 on the loss terms that evaluates against ground-truth reports $\mathcal{L}_{\text{unobs}}, \mathcal{L}_{\text{obs}}$.

Subsampled experiments: On both semi-synthetic and real data, we run subsampled experiments to compare the ratings-only model to the full model. We subsample ratings for each type individually. In Figure 3 (b) and Figure 4 (b) we report results for type k after subsampling ratings *only* for type k . One of the challenges of sparsity is that as ratings for type k become more sparsely observed, models learn noisier estimates of the true reporting coefficients θ_k, α_k . We address this challenge by (i) using two additional loss components and (ii) modifying how the model learns the reporting coefficients α_k, θ_k .

As a recap, we train all of our models with a loss function made up of four components: (i) report loss for data points with unobserved ratings, (ii) report loss for data points with observed ratings, (iii) rating loss, and (iv) regularization loss. For the models run on subsampled data, we also use:

(v) *Demographic coefficient regularization loss:* L^2 norm of the predicted demographic coefficients θ_k for the type k with subsampled ratings.

$$\mathcal{L}_{\theta\text{-reg}} = L^2(\theta_k) \quad (19)$$

Type frequency percentile	Correlation of ratings	
	Full model	Reports-only model
0-20%	0.269 ± 0.025	-0.074 ± 0.035
20-40%	0.197 ± 0.021	-0.066 ± 0.021
40-60%	0.367 ± 0.011	0.326 ± 0.007
60-80%	0.602 ± 0.005	0.581 ± 0.004
80-100%	0.768 ± 0.002	0.745 ± 0.002

Table 4: *The model can learn across types.* We evaluate our model’s performance in predicting ratings across type frequencies. We measure type frequency as $\mathbb{E}_{it} [T_{ikt}]$. Across all type frequency quintiles, and particularly for rare types (bottom quintiles), compared to the reports-only model, our full model, which uses both reporting and rating data, predicts more correlated ratings. We show results for all types that the model *does not* observe ratings for, and so the ratings-only model cannot be used at all. We report the mean and 95% CI across 20 synthetic datasets.

As ratings become increasingly sparse, we approach the setting of the reports-only model (where no ratings are observed). The reports-only model estimates ratings by using the estimated probability of observing a report $\hat{P}(T_{ikt})$ as a proxy for the rating. This loss component encourages a model to emulate the reports-only model by forcing the model’s predicted ratings \hat{r}_{ikt} to behave similarly to the model’s predicted probabilities of a report $\hat{P}(T_{ikt})$. In particular, this loss constrains the model’s ranking of the predicted ratings to match the model’s ranking of the predicted probabilities of a report by encouraging each predicted rating to be a scalar multiple of the predicted probability of a report (and not to additionally depend on demographics).

(vi) *ReLU penalty on rating coefficient:* Rectified linear unit (ReLU) penalty on the predicted rating coefficient α_k for the type k with subsampled ratings.

$$\mathcal{L}_{\alpha\text{-relu}} = \text{ReLU}(\alpha_k) \quad (20)$$

This loss component helps the model learn the inverse relationship (negative α_k coefficient) between ratings and reports – neighborhoods with lower ratings have worse conditions and therefore receive more reports. When ratings are sparsely observed, this relationship can be difficult to identify without this loss component.

Thus the overall loss is as follows:

$$\begin{aligned} \mathcal{L} = & \mathcal{L}_{\text{unobs}} + \gamma_1 \cdot \mathcal{L}_{\text{obs}} + \gamma_2 \cdot \mathcal{L}_{\text{rating}} + \gamma_3 \cdot \mathcal{L}_{\text{reg}} \\ & + \gamma_4 \cdot \mathcal{L}_{\theta\text{-reg}} + \gamma_5 \cdot \mathcal{L}_{\alpha\text{-relu}} \end{aligned} \quad (21)$$

We use weights $\gamma_1, \gamma_2, \gamma_3, \gamma_4, \gamma_5$ and fix the weight on $\mathcal{L}_{\text{unobs}}$ to 1.

For all models run on the full dataset, we use $\gamma_4 = \gamma_5 = 0$ (we use the $\gamma_1, \gamma_2, \gamma_3$ values specified earlier). For the ratings-only models run on subsampled data, we use the same hyperparameters as the ratings-only model run on the full dataset. Thus we use $\gamma_1 = 0, \gamma_2 = 1, \gamma_3 = 10^{-6}, \gamma_4 = 0, \gamma_5 = 0$. For the semi-synthetic experiments, the full model run on subsampled data uses $\gamma_1 = 20, \gamma_2 = 10, \gamma_3 = 10^{-6}, \gamma_4 = 0, \gamma_5 = 0$. For the real data experiments, the full model run on subsampled data uses $\gamma_1 = 20, \gamma_2 = 10, \gamma_3 = 10^{-6}, \gamma_4 = 0.1, \gamma_5 = 0.1$. Note that we only apply the two additional loss components for the full model run on subsampled real data. All other hyperparameters are identical to the standard model.

For the full model run on real subsampled data, we also modify how the model learns the reporting coefficients

α_k, θ_k . Our standard full model only learns the reporting coefficients α_k, θ_k for each type k with observed ratings using datapoints with observed ratings (see Case 1 in the model section). However, as ratings become more sparsely observed, we learn the reporting coefficients from fewer datapoints and therefore learn noisier estimates of α_k, θ_k . On the other hand, the reports-only model, which observes no ratings, learns reporting coefficients α_k, θ_k for all types k using all datapoints. While this introduces identifiability issues (since we are simultaneously learning ratings r_{ikt} and the coefficient on rating α_k), this improves our estimate of the demographic coefficients θ_k which can now be learned from the entire dataset (not just from datapoints with observed ratings). We use this intuition to modify our full model. We learn reporting coefficients for the type k with subsampled ratings using a weighted combination of gradients from datapoints with observed ratings and datapoints with unobserved ratings. We downweight gradients from datapoints with unobserved ratings using a weight of 0.6.

Further details on the semi-synthetic experiments

Semi-synthetic data

We generate synthetic inspection ratings r_{ikt} using eq. (9). We separately generate ratings for the train and test split. For example, for the train split, $\mathbb{E}_t(T_{ikt})$ is defined as the empirical frequency of T_{ikt} over all weeks in the train time period. We draw α_k and θ_k from a Gaussian. The mean of the Gaussian is calculated as follows: We take our real rating data, and separately for each type fit a logistic regression predicting reports from demographics and the ground-truth rating ($T_{ikt} \sim X_i, r_{ikt}$). We set the mean α_k and θ_k (other than the intercept) to be the average over the coefficients predicted across these type-specific logistic regressions. We set the intercept such that the ratings are zero mean. Thus, our generated and real inspection ratings take on both negative and nonnegative values.

Semi-synthetic results

We evaluate our predicted reports and ratings using both *correlation* and *root mean squared error (RMSE)*.

Correlation results: We evaluate reports by calculating the correlation between our model’s predicted probability of a report and the average true report across each node/type

Covariate	Mean coefficient
Bachelors degree population	0.234 ± 0.030
Households occupied by renter	0.174 ± 0.028
Median age	0.155 ± 0.010
log(Population density)	0.148 ± 0.035
White population	-0.072 ± 0.013
log(Median income)	-0.126 ± 0.024
True inspection rating	-0.193 ± 0.009

Table 5: *Multivariate reporting coefficients.* We report the average predicted multivariate demographic coefficients across types with observed ratings. The estimated coefficients capture known demographic factors: tracts that are more educated, older, or more dense are more likely to report incidents. We also report the coefficient on the true rating. Tracts that have lower ratings are more likely to be reported. We report the mean coefficients and 95% CIs over all contiguous two year periods between 2021 and 2023.

pair. In other words, we calculate $\text{corr}(\hat{P}(T_{ikt}), \mathbb{E}_t[T_{ikt}])$. We evaluate ratings by calculating the correlation between our models predicted rating and the average true rating across each node/type pair. In other words, we calculate $\text{corr}(\hat{r}_{ikt}, \mathbb{E}_t[r_{ikt}])$.

In Table 3, we calculate the average correlation on reports across all node/type pairs and the average correlation on ratings across node/type pairs with observed ratings. The ratings-only model only predicts ratings, so we cannot evaluate its performance on predicting reports. Similarly, the reports-only model only predicts probabilities of reports. Thus in order to estimate the reports-only model’s correlation on ratings we use the predicted probability of a report as a proxy for rating and evaluate $\text{corr}(\hat{P}(T_{ikt}), \mathbb{E}_t[r_{ikt}])$.

In Figure 3 (a), we calculate the correlation on reports for each type with observed ratings separately. In Table 4, we calculate the correlation on reports for each type with unobserved ratings. In both cases, compared to the reports-only model, we find that our full model predicts ratings that are more correlated with ground truth.

RMSE results: We evaluate reports by calculating the RMSE between our models predicted probability of a report and the average true report across each node/type pair. In other words, we calculate $\text{RMSE}(\hat{P}(T_{ikt}), \mathbb{E}_t[T_{ikt}])$. We evaluate ratings by calculating the RMSE between our model’s predicted rating and the average true rating across each node/type pair. In other words, we calculate $\text{RMSE}(\hat{r}_{ikt}, \mathbb{E}_t[r_{ikt}])$.

In Table 3, we calculate the average RMSE on reports across all node/type pairs and the average RMSE on ratings across node/type pairs with observed ratings. We report the mean RMSE across 20 synthetic datasets. We note that the ratings-only model only predicts ratings. Therefore, we cannot evaluate its performance on predicting reports. Similarly, the reports-only model only predicts probabilities of reports. Therefore, we cannot evaluate its performance on predicting ratings. Note that unlike for correlation, when calculating RMSE, we *cannot* use a proxy for rating (e.g., $\hat{P}(T_{ikt})$).

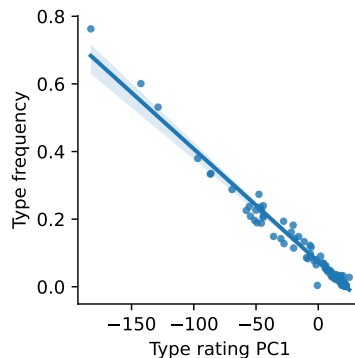


Figure 6: *The model learns interpretable ratings.* Each type’s learned ratings over nodes capture type frequency information. In particular, the dimension of highest variance of our type ratings (PC1) has a high correlation with type reporting frequency $\mathbb{E}_k [T_{ikt}]$.

Discussion of reports-only model’s results: We now discuss the reports-only model’s results in more detail. As seen in Table 3, the reports-only model can predict the probability of a report $P(T_{ikt})$ well ($r = 0.48$). However, compared to the full model, the reports-only model predicts ratings that are poorly correlated with ground truth ($r = 0.62$ for the full model versus 0.33 for the reports-only model). In the semi-synthetic data, ratings are produced by eq. (9). In order to produce well-calibrated ratings, we must recover the true empirical frequencies $\mathbb{E}_t(T_{ikt})$ and the true type-specific demographic coefficient θ_k .⁴ We claim that the reports-only model is unable to predict well-correlated ratings because it cannot recover the true demographic coefficient θ_k . We show this is true by comparing the reports-only model’s rating predictions to ratings calculated according to eq. (9) using the *true* value of θ_k and with $\mathbb{E}_t(T_{ikt})$ equal to the reports-only model’s estimates of $P(T_{ikt})$. In the latter case, our predicted ratings are better correlated with the true synthetic ratings ($r = 0.53$ versus 0.33 for the reports-only model). This improvement is solely due to correcting the value of the demographic coefficient θ_k . We note that despite the improvement, the correlation $r = 0.53$ is still below that of the full model (0.62). This is because for data points with observed ratings the full model produces better estimates of $P(T_{ikt})$ ($r = 0.57$ for the full model versus 0.50 for the reports-only model). Overall we have shown that the reports-only model’s ratings are poorly correlated with the ground-truth ratings because it *cannot* recover the true demographic coefficients θ_k . Only a model which observes ratings can accurately recover θ_k , therefore even though the reports-only model can accurately predict $\mathbb{E}_t(T_{ikt})$ it is fundamentally limited in its rating predictions.

Further details on the real-world case study

Real data results: We report our model’s correlation and RMSE on predicted reports and ratings in Table 3.

⁴We *do not* need to recover the type-specific rating coefficient α_k to produce *well-calibrated* ratings, we only need to recover α_k if we want to *exactly* recover ratings.

Cluster	0	1	2	3
Race:Non-Hispanic White	29%	55%	12%	35%
Race:Asian	18%	16%	5%	18%
Race:African-American	19%	8%	35%	21%
Households occupied by renter	59%	72%	87%	45%
Bachelors degree	33%	71%	26%	36%
Population	3,900	5,600	5,200	2,600
Median income	71,000	120,000	47,000	74,000
Median age	38	37	35	40

Table 6: *Clustered nodes are demographically distinct.* We find that the clustering correlates with differences in demographics. All differences between clusters are statistically significant ($p < 0.001$, ANOVA test). The largest value in each row is shown in bold.

Predicted demographic coefficients: In Table 1 we report the demographic coefficients predicted by univariate models. In Table 5 we report the demographic coefficients predicted by a multivariate model.

Clustered nodes are demographically distinct: For each node i , we create a vector $\mathbf{r}_i = \{r_{ikt}\}_{k=1}^T$ of ratings over all types k . We use each node’s \mathbf{r}_i vector to cluster the nodes into 4 groups. We find that the predicted clusters are spatially correlated and demographically distinct. We report the statistically significant differences in demographics for each cluster in Table 6.

Clustering ratings for each type: For each type k , we create a vector $\mathbf{r}_k = \{r_{ikt}\}_{i=1}^n$ of ratings over all nodes i to cluster the types into 8 groups. We find that each group contains a coherent cluster of types, and in Table 7 we describe and list the types captured by each cluster. Additionally, Figure 6 shows that the dimension of highest variability (i.e., first PCA dimension) of the \mathbf{r}_k vectors captures type frequency (i.e., $\mathbb{E}_{it}[T_{ikt}]$).

Table 7: *Ratings capture correlations between 311 complaint types.* Using each type’s vector of learned ratings over nodes, we cluster types into 8 groups using a k means clustering algorithm. We manually assign a succinct cluster description to each group. We find that the clusters group similar types together.

Cluster Description	Complaint Types
Housing Maintenance	Appliance (HPD) Door/Window (HPD) Electric (HPD) Flooring/Stairs (HPD) General (HPD) Paint/Plaster (HPD) Plumbing (HPD) Water Leak (HPD)
Residential Complaints	Street Light Condition (DOT) Missed Collection (DSNY) Heat/Hot Water (HPD) Unsanitary Condition (HPD) Blocked Driveway (NYPD) Illegal Parking (NYPD) Noise - Residential (NYPD) Noise - Street/Sidewalk (NYPD)
Public Space Nuisances	Noise (DEP) Water System (DEP) General Construction/Plumbing (DOB) Derelict Vehicles (DSNY) Dirty Condition (DSNY) Illegal Dumping (DSNY) Abandoned Vehicle (NYPD) Noise - Commercial (NYPD) Noise - Vehicle (NYPD)
Public Health and Landscape	Sewer (DEP) Building/Use (DOB) Rodent (DOHMH) Sidewalk Condition (DOT) Damaged Tree (DPR) Dead/Dying Tree (DPR) New Tree Request (DPR) Overgrown Tree/Branches (DPR) Root/Sewer/Sidewalk Condition (DPR) Dead Animal (DSNY) Electronics Waste Appointment (DSNY) Obstruction (DSNY)
Safety and Mobility Issues	Consumer Complaint (DCA) Encampment (DHS) Homeless Person Assistance (DHS) Elevator (DOB) Outdoor Dining (DOT) Traffic Signal Condition (DOT) Encampment (NYPD) Non-Emergency Police Matter (NYPD) Panhandling (NYPD) For Hire Vehicle Complaint (TLC) Lost Property (TLC) Taxi Complaint (TLC)

Cleanliness and Safety
Concerns

Asbestos (DEP)
Hazardous Materials (DEP)
Water Quality (DEP)
BEST/Site Safety (DOB)
Electrical (DOB)
School Maintenance (DOE)
Construction Lead Dust (DOHMH)
Face Covering Violation (DOHMH)
Non-Residential Heat (DOHMH)
Standing Water (DOHMH)
Unleashed Dog (DOHMH)
Unsanitary Animal Pvt Property (DOHMH)
Unsanitary Pigeon Condition (DOHMH)
Broken Parking Meter (DOT)
Abandoned Bike (DSNY)
Commercial Disposal Complaint (DSNY)
Dumpster Complaint (DSNY)
Illegal Posting (DSNY)
Litter Basket Complaint (DSNY)
Litter Basket Request (DSNY)
Lot Condition (DSNY)
Snow or Ice (DSNY)
Noise - Helicopter (EDC)
Elevator (HPD)
Bike/Roller/Skate Chronic (NYPD)
Drinking (NYPD)
Drug Activity (NYPD)
Graffiti (NYPD)
Urinating in Public (NYPD)
Taxi Report (TLC)

Infrastructure and
Environmental Health

Consumer Complaint (DCWP)
Air Quality (DEP)
Lead (DEP)
Water Conservation (DEP)
Boilers (DOB)
Emergency Response Team (ERT) (DOB)
Plumbing (DOB)
Real Time Enforcement (DOB)
Special Projects Inspection Team (SPIT) (DOB)
Food Establishment (DOHMH)
Indoor Air Quality (DOHMH)
Smoking (DOHMH)
Curb Condition (DOT)
Street Condition (DOT)
Street Sign - Damaged (DOT)
Street Sign - Dangling (DOT)
Street Sign - Missing (DOT)
Animal in a Park (DPR)
Illegal Tree Damage (DPR)
Maintenance or Facility (DPR)
Violation of Park Rules (DPR)
Graffiti (DSNY)
Residential Disposal Complaint (DSNY)
Sanitation Worker or Vehicle Complaint (DSNY)
Street Sweeping Complaint (DSNY)
Safety (HPD)
Animal-Abuse (NYPD)

	Illegal Fireworks (NYPD) Noise - Park (NYPD) Traffic (NYPD)
Facility and Health Inspections	Industrial Waste (DEP) AHV Inspection Unit (DOB) Investigations and Discipline (IAD) (DOB) Scaffold Safety (DOB) Asbestos (DOHMH) Beach/Pool/Sauna Complaint (DOHMH) Day Care (DOHMH) Drinking Water (DOHMH) Harboring Bees/Wasps (DOHMH) Illegal Animal Kept as Pet (DOHMH) Indoor Sewage (DOHMH) Mold (DOHMH) Mosquitoes (DOHMH) Pet Shop (DOHMH) Poison Ivy (DOHMH) Tattooing (DOHMH) Bike Rack Condition (DOT) Bus Stop Shelter Complaint (DOT) Bus Stop Shelter Placement (DOT) E-Scooter (DOT) Uprooted Stump (DPR) Wood Pile Remaining (DPR) Adopt-A-Basket (DSNY) Seasonal Collection (DSNY) Water System (NYC311-PRD) Disorderly Youth (NYPD) Noise - House of Worship (NYPD) For Hire Vehicle Report (TLC) Green Taxi Complaint (TLC)